40673-MC

AD650633

WESTINGHOUSE ELECTRIC CORPORATION
Research Laboratories
Pittsburgh, Pennsylvania 15235

Project Number: ARO-D-196

Final Report

STUDIES ON THE HIGH TEMPERATURE OXIDATION OF MOLYBDENUM, TUNGSTEN, NIOBIUM, TANTALUM, TITANIUM, AND ZIRCONIUM

Contract Number: DA-31-124-ARO-D-196

April 18, 1967

E. A. Gulbransen
K. F. Andrew
F. A. Brassart

D D C
APR 26 1967
A

DISTRIBUTION OF THIS DOCUMENT IS UNLIMITED

ARCHIVE COPY

69

WESTINGHOUSE ELECTRIC CORPORATION
Research Laboratories
Pittsburgh, Pennsylvania 15235

Project Number: ARO-D-196

Final Report

STUDIES ON THE HIGH TEMPERATURE OXIDATION OF MOLYBDENUM, TUNGSTEN, NIOBIUM, TANTALUM, TITANIUM, AND ZIRCONIUM

Contract Number: DA-31-124-ARO-D-196

April 18, 1967

E. A. Gulbransen
K. F. Andrew
F. A. Brassart

DISTRIBUTION OF THIS DOCUMENT IS UNLIMITED

STUDIES ON THE HIGH TEMPERATURE OXIDATION OF
MOLYBDENUM, TUNGSTEN, NIOBIUM, TANTALUM,
TITANIUM, AND ZIRCONIUM

General Introduction and Purpose

1. Vacuum Microbalance Methods for Studying Fast Gas-Metal Reactions

   1.1 Introduction

   1.2 Static and Flow Reaction Systems

2. Oxidation of Rhenium and a Rhenium-8% Titanium Alloy at Oxygen Pressure of 1 to 10 Torr and at 800° to 1400°C in Flow Environments

   2.1 Introduction

   2.2 Literature

   2.3 Experimental

   2.4 Results

   2.5 Discussion of the Mechanism of Oxidation

      2.5.1 Absolute Reaction Rate Theory

      2.5.2 Flow and Kinetic Theory Efficiencies

3. Oxidation of Molybdenum in Flow Environments at Temperatures of 900° to 1600°C and at Oxygen Pressures of 9×10^{-3} to 49 Torr

   3.1 Introduction

   3.2 Experimental

   3.3 Method

   3.4 Results

   3.5 Discussion of Mechanisms

      3.5.1 Efficiency Calculations

      3.5.2 Absolute Reaction Rate Theory

4. Thermochemical Analyses on the Oxidation of Molybdenum

5. High Voltage Electron Diffraction Apparatus for Studying Oxidation Reactions at Pressure, at Temperature and under Flow Conditions

5.1 Introduction

5.2 Electron Diffraction Camera

5.3 Strip Heater Furnace and Reaction Chamber

5.4 Test of Gas Handling System

5.5 Determination of Instrument Constant

5.6 Results

5.6.1 Test Study on Rhombohedral α-Fe_2O_3

5.6.2 Study of Molybdenum Oxidation

6. Summaries of Recent Scientific Papers

6.1 The Graphite-Hydrogen Reactions and Their Implications in Geochemistry

6.2 Nature of the Reaction Products Formed in the Graphite-Hydrogen Reaction at 1300°-1400°C

6.3 Oxidation of Silicon at High Temperatures and Low Pressures under Flow Conditions and the Vapor Pressure of Silicon

6.4 Oxidation of Silicon Carbide at 1150° to 1400°C and at 9×10^{-3} to 5×10^{-1} torr Oxygen Pressure

7. List of Publications and Technical Reports

8. List of Participating Scientific Personnel

GENERAL INTRODUCTION AND PURPOSE

The purpose of these studies was twofold: (1) to extend and develop vacuum microbalance and electron diffraction methods for studying fast oxidation reactions of high temperature metals and solids under carefully controlled conditions of temperature, pressure, and gas flow; and (2) to determine the kinetics and mechanisms of oxidation of a number of high temperature metals and solids.

The oxidation resistance of the highest melting point and lowest volatility elements, tungsten, molybdenum, rhenium, and carbon, is not controlled by the transport of reacting species through an oxide scale or film since volatile oxides are formed at high temperatures. Other materials, such as silicon, silicon carbide, and molybdenum disilicide can take on passive or active properties depending on the reaction conditions.

For some reaction conditions adsorption of oxygen, desorption of the oxide, or chemical reaction of the adsorbed species limits the kinetics of oxidation. For other conditions the diffusion of oxygen molecules through a barrier layer of volatilized oxide vapors limits the rate of oxidation of these elements. The transition between chemical controlled reaction mechanisms and gas diffusion of oxygen through the volatilized gases must be studied.

High temperature materials for many energy producing and space devices are under severe flow conditions. Flow can accelerate gas-solid reactions by removing the reaction products so that normal equilibrium conditions are not achieved and by removing the barrier layers of oxide vapors which may limit access of oxidizing gases to the surface.

The nature of the reaction interface between the metal and the oxidizing gas, under reaction conditions, is very important in determining the mechanism of the reaction. Similarly, the nature of the reacting gases whether molecular or atomic is important. The equilibrium between atomic and molecular oxygen can be calculated from free energy data.

The work performed under the present contract will be given under the following headings:

1. Vacuum microbalance apparatus and methods
2. Kinetic studies on the oxidation of rhenium
3. Kinetic studies on the oxidation of molybdenum
4. Thermochemical studies on the oxidation of molybdenum
5. Summaries of other kinetic studies
6. Electron diffraction apparatus and method
7. Electron diffraction studies on the oxidation of molybdenum

1. VACUUM MICROBALANCE METHODS FOR STUDYING FAST GAS-METAL REACTIONS

1.1 Introduction

Both static and dynamic or flow type of reaction systems can be used to measure the wide variety of chemical reactions occurring on metal surfaces. Both systems can be incorporated in a single apparatus. A static reaction system is one where no external flow is imposed on the system. Some gas circulation occurs as a result of thermal gradients along the furnace tube. If such a system is operated at constant pressure, the make-up gas as well as the weight change can be used to evaluate the kinetics of complex oxidation reactions.

A flow reaction system is one in which external gas flow is imposed on the system which is usually at atmospheric pressure. Flow systems operating at pressures below atmospheric require careful control of the gas source and the exhaust pump in order to maintain a constant pressure in the system.

Weight change methods using various types of microbalances have been used in both static and dynamic reaction systems. These methods have been developed extensively during the past six years. Oxygen consumption methods should become more useful in the future with the recent development of sensitive quartz type of Bourdon gauges and the sensitive types of constant temperature capacity manometers. Capacity manometers sensitive to 1 in 10^5 are now available. Thermal conductivity and gas analysis methods have also been developed extensively.

1.2 Static and Flow Type Reaction Systems

In a static reaction system operating at constant pressure, both weight change and oxygen consumption methods are used to follow the course of a gas-solid reaction. Where both oxide films and volatile oxides are f[illegible] the two methods make possible the determination of both oxide film formation and oxide volatility.[1][2] When oxygen consumption is to be measured, it is necessary to keep the volume of the reaction and measuring systems to 1 liter or less so as to improve the precision of pressure control.

Figure 1 shows the balance housing, furnace tube and associated reaction system. Various types of balances having an overall beam length of 14.5 cm and sensitivities as low as 1 μg/0.001 cm deflection at 7.25 cm can be used. Some of these balances have been described in earlier papers.[3][4]

Figure 2 shows a gold plated Invar beam balance[5] designed for the study of fast reactions and occupying a small volume. The sensitivity and period can be varied by positioning movable beam weights which are not shown in Figure 2. The beam weighs 46 g, has a period of about 2 seconds and in one modification a sensitivity of 75 μg/0.001 cm at 7.25 cm distance and for a weight of 1.4 g.

---

1. E. A. Gulbransen, K. F. Andrew and F.A. Brassart, J. Electrochem. Soc. 110, 476 (1963).
2. E. A. Gulbransen, K. F. Andrew and F. A. Brassart, J. Electrochem. Soc. 110, 952 (1963).
3. E. A. Gulbransen, Rev. Sci. Instr. 15, 201 (1944).
4. E. A. Gulbransen and K. F. Andrew, in: M. J. Katz (ed) Vacuum Microbalance Techniques, Vol. 1, Plenum Press, New York, 1961, p. 1.
5. E. A. Gulbransen and K. F. Andrew, in: R. F. Walker (ed) Vacuum Microbalance Techniques, Vol. 2, Plenum Press, New York, 1962, p. 129.

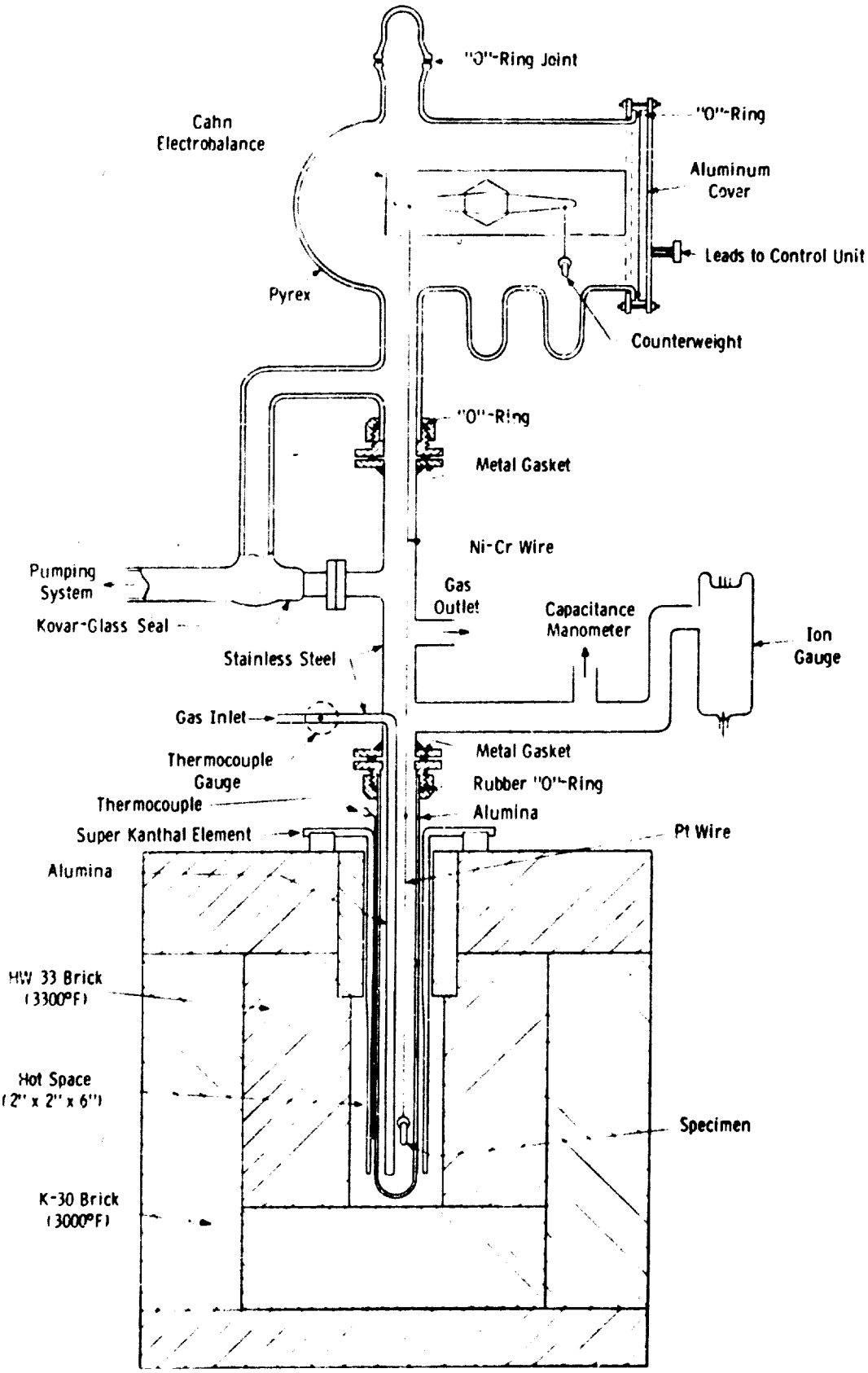

Fig. 1—Reaction System

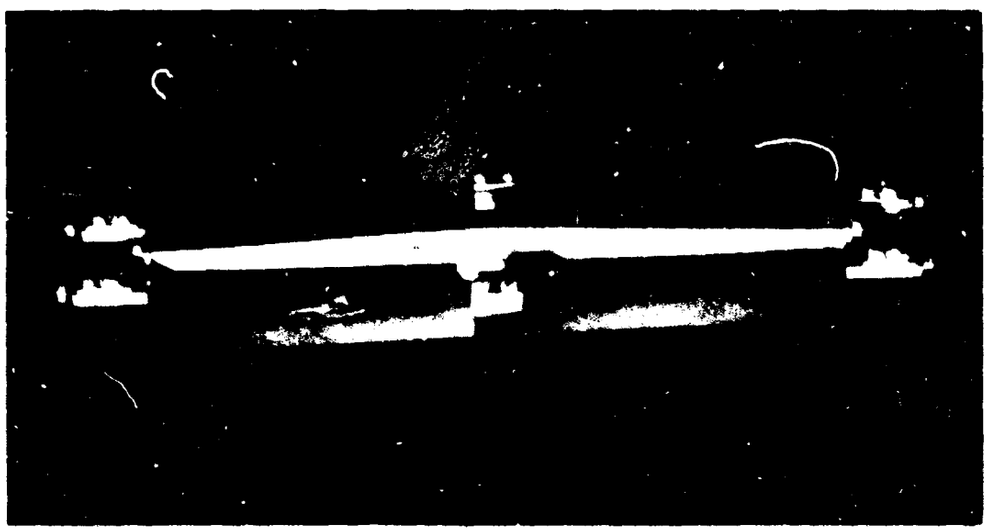

Fig. 2—Invar Balance

Specimens were suspended from the balance using platinum wire in the hot zone and 2 mil nickel-chromium wire in the cold zone. Above 1500°C platinum wire was unsatisfactory for supporting many materials. Silica or alumina fibers can be used above 1500°C for the support of some materials. Reaction between oxides and metals can occur. Special care must be used in choice of the support system.

The furnace tube shown in Figure 1 was a one inch diameter high density mullite or zircon tube These materials can be sealed directly to glass.[6] Alumina tubes were used for temperatures above 1200°C. One of the critical problems in the design of practical reaction systems is the furnace design. Figure 3 shows a special high temperature furnace using molybdenum disilicide furnace elements. The high temperature properties of molybdenum disilicide and a high temperature furnace design has been described.[7] Using 2 six inch S-306 Kanthal elements having an available power of 880 watts each, furnaces can be readily built to operate at temperatures up to 1650°C. One set of furnace elements was in use every day for 3 years at temperatures between 1000° and 1650°C. Calibrated Pt-Pt + 10% Rh thermocouples were used within the furnace tube or attached externally to the furnace tube. The temperature of the furnace could be established by adjusting the current in the heater elements.

Figure 4 shows a schematic diagram of the vacuum system, gas preparation trains, and the system for measuring oxygen consumption. The vacuum system was not bakeable. The residual pressure obtainable at room temperature was 10^{-6} torr. The pressure in the system was automatically controlled by a Granville Philips pressure control system. For pressures above 0.1 torr, a capacity manometer was used as a pressure sensor, and for pressures below 10^{-4} an ion gauge was used as a pressure sensor. For intermediate pressures of 10^{-4} to 10^{-1} torr the ion gauge

6. E. A. Gulbransen and K. F. Andrew, Ind. Eng. Chem. 41, 2762 (1949).
7. E. A. Gulbransen, K. F. Andrew and F. A. Brassart, in: K. H. Behrndt (ed) Vacuum Microbalance Techniques, Vol. 3, Plenum Press, New York, 1963, p. 179.

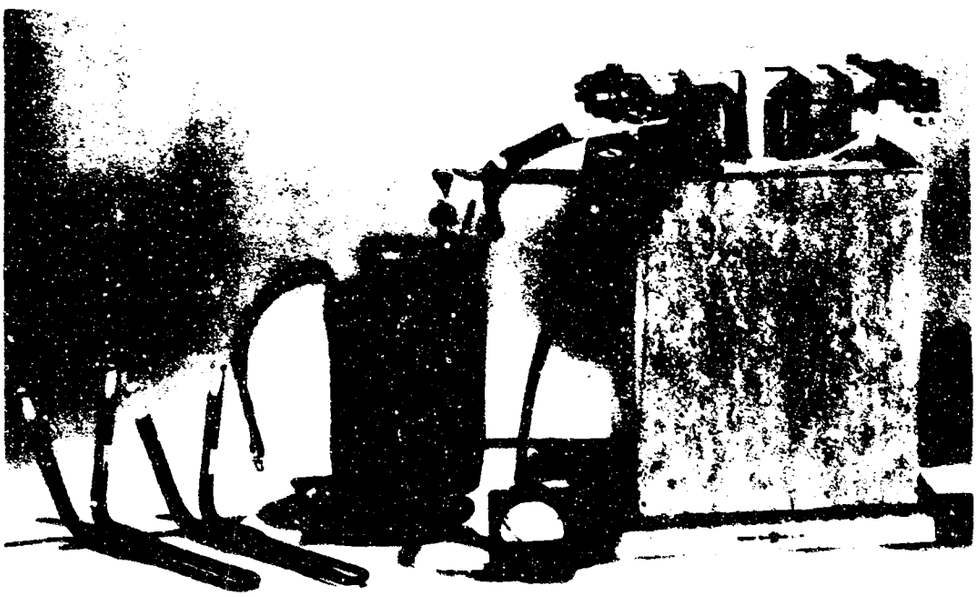

Heating Elements Transformer Furnace

Fig. 3—Kanthal furnace

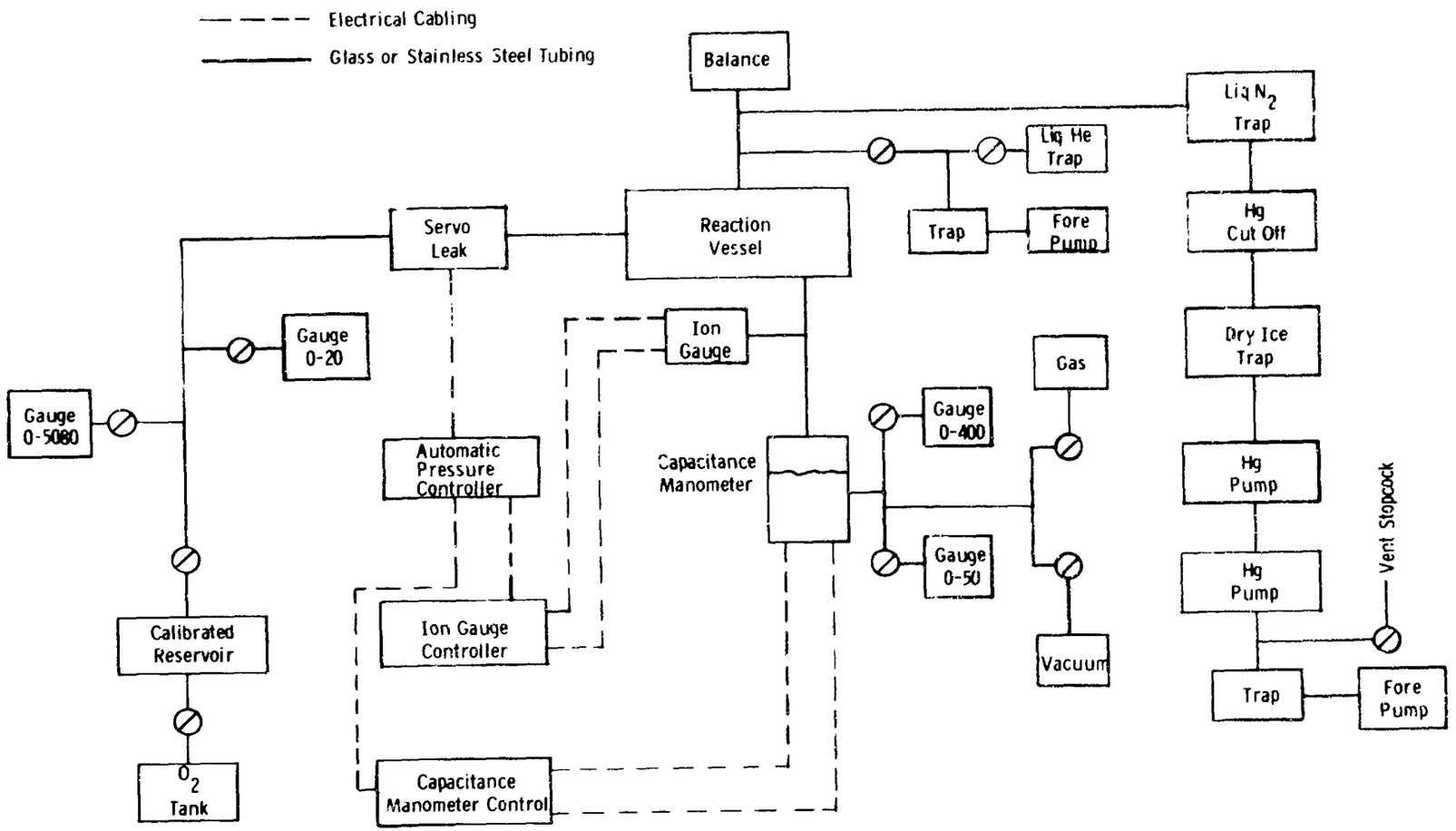

Fig. 4—Schematic diagram of vacuum microbalance system

can be used as a Pirani gauge type pressure sensor. The Pirani gauge function has not been successfully used as of this date. The several pressure sensors were used to control the opening of a sensitive leak valve to adjust the pressure in the system to the desired value. The amount of gas used was measured by reading the pressure on a calibrated reservoir. Two sensitive Wallace-Tiernan pressure gauges were used to measure the pressure in the reservoir. Using a 2.6 liter reaction system and controlling the pressure to 10^{-1} torr, oxygen consumption could be measured to $\pm 4 \times 10^{-4}$ g. This sensitivity could be improved by using a more accurate capacity manometer, by reducing the volume of the reaction system and by improving the pressure readout on the calibrated reservoir.

For the flow type reaction system a fore pump is activated and the pumping speed varied by an adjustable orifice. By control of the fore pump speed and the servo leak, the flow rate of gas over the specimen can be regulated and measured.

2. OXIDATION OF RHENIUM AND A RHENIUM-8% TITANIUM ALLOY AT OXYGEN PRESSURES OF 1 TO 10 TORR AND AT 800° TO 1400°C IN FLOW ENVIRONMENTS

2.1 Introduction

Carbon, rhenium, molybdenum, and tungsten are some of the best high temperature elements. Each forms a volatile oxide when oxidized above a certain critical temperature. Above the temperature for formation of volatile oxides, thick oxide films are absent from the metal surface and fast chemical reactions occur. For these conditions chemical reaction of oxygen molecules or atoms occurs with the metal interface or with a thin layer of non-volatile lower oxide. At some temperature diffusion of oxygen gas through a barrier layer of volatilized oxide occurs.

Experimentally, rhenium is one of the best metals for studying high temperature oxidation processes. Although rhenium has a melting point of 3967 $\pm$ 60°C and a boiling point of about 5900°C (est.), the oxide Re_2O_7 melts at 296°C and boils at 362°C. The metal can be obtained in a dense form and in a relatively pure state.

Rhenium forms the volatile oxide Re_2O_7 during oxidation. Thick oxide films are absent on the metal and fast oxidation reactions can occur. These fast oxidation reactions may be controlled by chemical processes such as adsorption and desorption and by gas diffusion of oxygen through a barrier layer of volatilized Re_2O_7. The chemical processes can be distinguished from gas diffusion controlled processes by a careful study of the temperature and pressure coefficients of the rates of reaction and the effect of sample size or flow on the rates of reaction.

2.2 Literature

The oxidation of rhenium has not been studied extensively. Lavrenko[8] studied the oxidation of 99.94% Re over the temperature range of 350°-750°C. Linear oxidation rates were observed. Phillips[9] has reviewed recent work and has extended the oxidation studies to 1300°C. Linear oxidation rates were observed for air oxidation. The oxide formed was Re_2O_7.

2.3 Experimental

A flow reaction system[10] was used for all of the kinetic measurements. The pure rhenium specimens were right cylinders having surface areas of about 0.75 cm^2 whereas the rhenium-8% titanium specimens were rectangular plates having surface areas of about 0.6 cm^2. The specimens were suspended from one end of a sensitive microbalance that was enclosed in the vacuum and reaction system. The balance was a recording type electrobalance having a sensitivity of 10^{-7} g/mm change on the recorder chart, a period of less than 0.1 sec, a load capacity of 1 g and a range of 1 g. The oxygen gas was preheated, led to the bottom of the furnace and exhausted at the top of the furnace tube. The gas handling system was automated to control the pressure and gas flow rate by using a servo-operated leak valve. Pressures of 1 to 10 torr were used. Gas was added manually and after the desired pressure was achieved the reaction system was switched to automatic control. Reliable readings on the recorder chart were obtained after 10-30 seconds of elapsed time.

---

8. V. O. Lavrenko, Dopovidi Akad. Nauk. R.S.R., pp. 1216-20 (1958).
9. W. L. Phillips, Jr., J. Less Common Metals 5, 2, 97 (1963).
10. E. A. Gulbransen, K. F. Andrew and F. A. Brassart, in: P. M. Waters (ed) Vacuum Microbalance Techniques, Vol. 4, Plenum Press, New York, 1965, p. 127.

To minimize the formation of films of non-volatile impurities on the surface, high purity metal and high purity oxygen must be used. Reagent grade oxygen having 8.4 ppm N_2, 20 ppm CH_4 and 15.2 ppm Kr was used. The rhenium was obtained from Materials Research Corp. and had a purity of 99.999%.

2.4 Results

Figure 5 shows a typical weight loss vs. time curve for the oxidation of the Re-8% Ti alloy at 1400°C and 5 torr oxygen pressure. Figure 5 shows the weight loss to be a linear function of time. An initial buoyancy correction of 2.5 mg was found for the gas flow of 172 cm/sec. The gas flow rate was calculated from pressure readings on a standard volume of gas. An oxidation rate of 3.37×10^{-4} g of Re/cm^2-sec was found. This is 1.09×10^{18} atoms of Re reacting/cm^2-sec/ The flow rate calculated as O_2 molecules was 1.84×10^{19} molecules/sec.

The oxidation of high purity rhenium was studied at 1, 2, 5, and 10 torr for the temperature range of 600°-1400°C. The oxidation of the alloy was studied at 2 and 5 torr for the temperature range of 600°-1507°C.

Figure 6 shows a log weight change versus 1/T plot for the kinetic data on the oxidation of pure rhenium. Parallel straight lines were obtained for 2, 5, and 10 torr pressures below 1000° or 1100°C. For this region an enthalpy of activation of 16.8 kcal/mole was obtained. Above 1100°C a break occurs in the plot for 2, 5, and 10 torr oxygen pressures. The kinetic data below 1100°C can be considered as under control of chemical factors such as adsorption, desorption or chemical reaction. At about 1100°C a transition occurs to gas diffusion controlled rate processes. This was probably the diffusion of oxygen molecules through the volatilized oxide to the reaction interface. The temperature coefficient for this region is small. A summary of the kinetic data is given in Table 1.

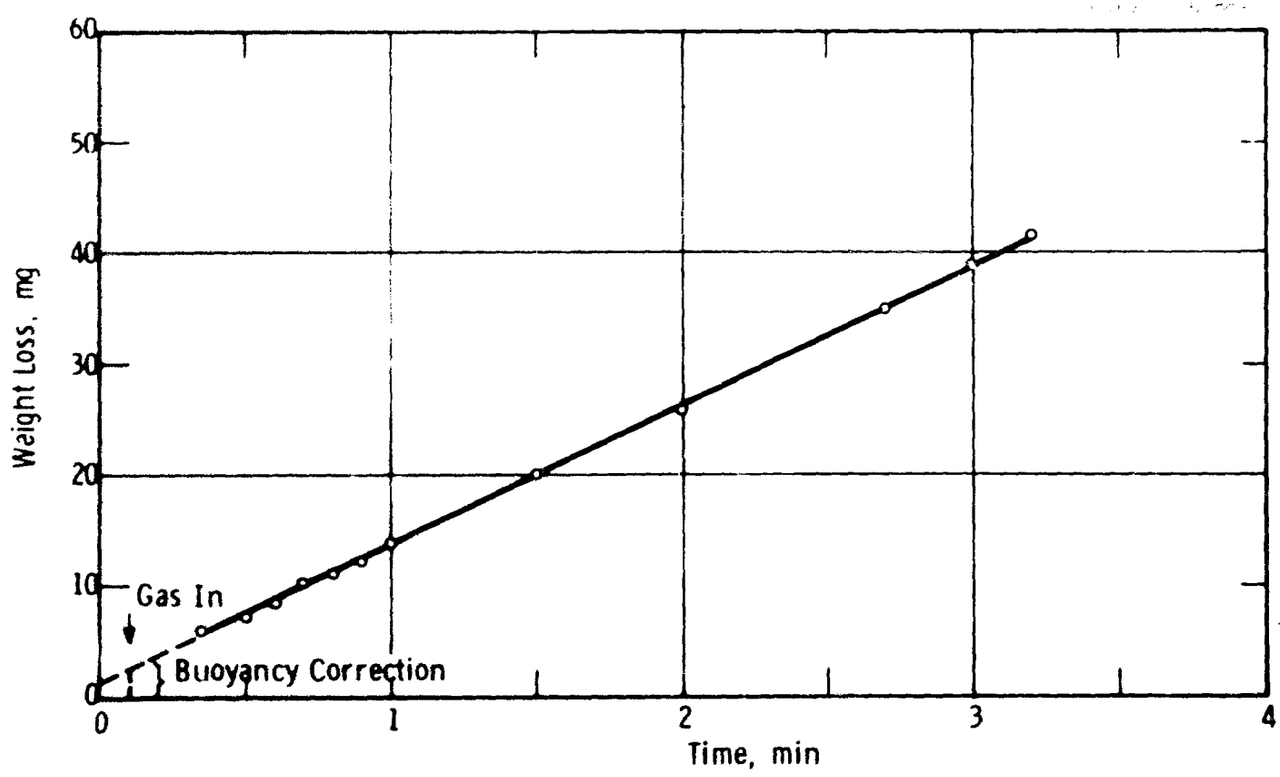

Fig. 5—Weight loss vs time, oxidation Re-8% Ti, 1400° C - 5 torr, flow 1.84×10^{19} O_2 molecules/sec

Curve 580056

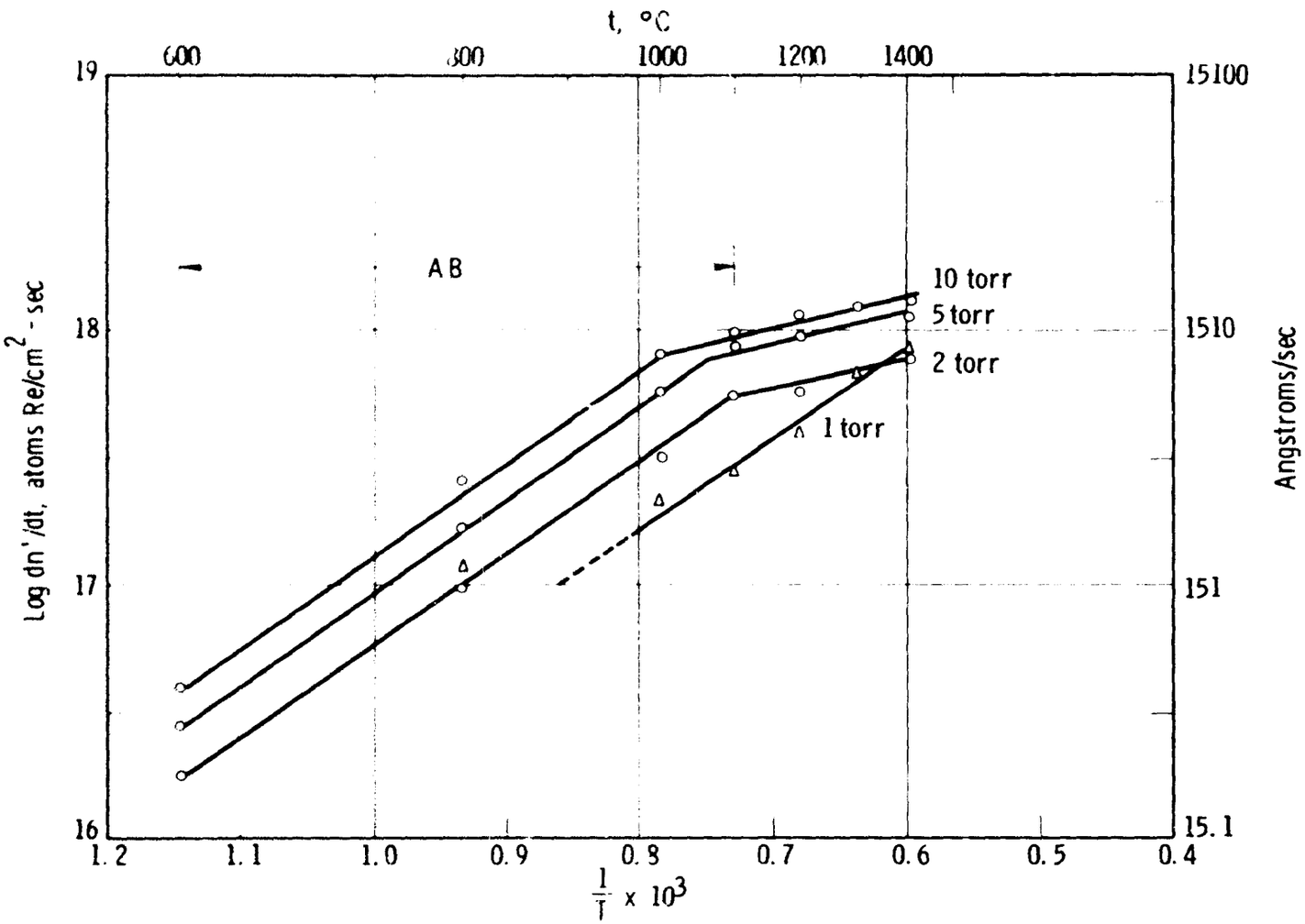

Fig. 6—Log dn'/dt vs $\frac{1}{T}$, oxidation of Rhenium, 600°-1400°C, flow 0.42-1.95 x 10^{19} O_2, molecules/sec

Table 1

Kinetic Data Oxidation of Rhenium 600° to 1400°C

Pressure torr	Temp. °C	Area cm^2	Gas Flow O atoms/sec	dw'/dt g/cm^2-sec	dn'/dt atoms Re/cm^2-sec	log dn'/dt
1	800	.674	2.57×10^{19}	3.64×10^{-5}	1.17×10^{17}	17.068
1	1000	.702	2.65×10^{19}	6.44×10^{-5}	2.08×10^{17}	17.318
1	1100	.708	2.74×10^{19}	8.47×10^{-5}	2.74×10^{17}	17.438
1	1200	.715	2.69×10^{19}	1.20×10^{-4}	3.87×10^{17}	17.588
1	1300	.727	2.69×10^{19}	2.10×10^{-4}	6.80×10^{17}	17.833
1	1400	.743	2.78×10^{19}	2.52×10^{-4}	8.15×10^{17}	17.911
2	600	.640	8.39×10^{18}	5.34×10^{-6}	1.73×10^{16}	16.238
2	800	.640	8.70×10^{18}	2.93×10^{-5}	9.46×10^{16}	16.976
2	1000	.730	9.62×10^{18}	9.53×10^{-5}	3.08×10^{17}	17.489
2	1100	.645	9.96×10^{18}	1.67×10^{-4}	5.40×10^{17}	17.732
2	1200	.707	9.96×10^{18}	1.71×10^{-4}	5.53×10^{17}	17.743
2	1300	.665	9.96×10^{18}	2.12×10^{-4}	6.83×10^{17}	17.834
2	1400	.685	9.96×10^{18}	2.29×10^{-4}	7.40×10^{17}	17.869
5	600	.639	3.56×10^{19}	8.63×10^{-6}	2.78×10^{16}	16.444
5	800	.637	3.56×10^{19}	5.10×10^{-5}	1.64×10^{17}	17.215
5	1000	.625	3.68×10^{19}	1.96×10^{-4}	5.53×10^{17}	17.743
5	1100	.575	3.73×10^{19}	2.63×10^{-4}	8.50×10^{17}	17.929
5	1200	.615	3.79×10^{19}	2.83×10^{-4}	9.15×10^{17}	17.961
5	1400	.600	3.69×10^{19}	3.37×10^{-4}	1.09×10^{18}	18.037
10	600	.725	1.37×10^{19}	1.16×10^{-6}	3.74×10^{16}	16.573
10	800	.730	1.66×10^{19}	7.84×10^{-5}	2.53×10^{17}	17.403
10	1000	.680	3.11×10^{19}	2.39×10^{-4}	7.70×10^{17}	17.886
10	1100	.607	3.85×10^{19}	2.95×10^{-4}	9.54×10^{17}	17.979
10	1200	.580	3.90×10^{19}	3.44×10^{-4}	1.11×10^{18}	18.045
10	1300	.560	3.81×10^{19}	3.71×10^{-4}	1.20×10^{18}	18.079
10	1400	.540	3.81×10^{19}	4.00×10^{-4}	1.29×10^{18}	18.111

Figure 7 shows a similar plot for the Re-8% Ti alloy for 2 and 5 torr oxygen pressure. The log dn'/dt vs. 1/T plots in Figure 7 were similar to those for rhenium except in the low temperature region 600°-1000°C which shows a steeper slope, i.e. greater enthalpy of activation, 21 kcal/mole. The transition between chemical controlled oxidation and gas diffusion controlled oxidation occurs at or about 1100°C. The rates of oxidation at high temperatures were similar to those obtained with the pure metal. Figure 8 shows a comparison of the rate data for high purity rhenium and the Re-8% Ti alloy at 5 torr oxygen pressure.

2.5 Discussion of the Mechanism of Oxidation

2.5.1 Absolute Reaction Rate Theory

Eyring and coworkers[11] have developed rate equations for the several types of surface reactions including mobile adsorption, chemical reaction, and desorption. The Eyring and coworkers' expression for mobile adsorption is

$$dn'/dt = S/\ell \, C_g kT \times (2\pi mkT)^{-1/2} \times \exp(-\Delta H_1/RT) \qquad (1)$$

Where dn'/dt is the rate of reaction in atoms of Re/cm^2-sec, ℓ is the stoichiometric factor, S is the surface area/cm^2, C_g is the concentration of O_2 molecules per cubic centimeter in the gas phase, k, Boltzmann's constant, T, absolute temperature, and ΔH_1, enthalpy of activation. Work in our laboratory has shown that mobile adsorption is probably the rate controlling step in the oxidation of carbon[1] and of molybdenum.[2]

---

11. K. J. Laidler, S. Glasstone and H. Eyring, J. Chem. Phys. 8, 659 (1940).

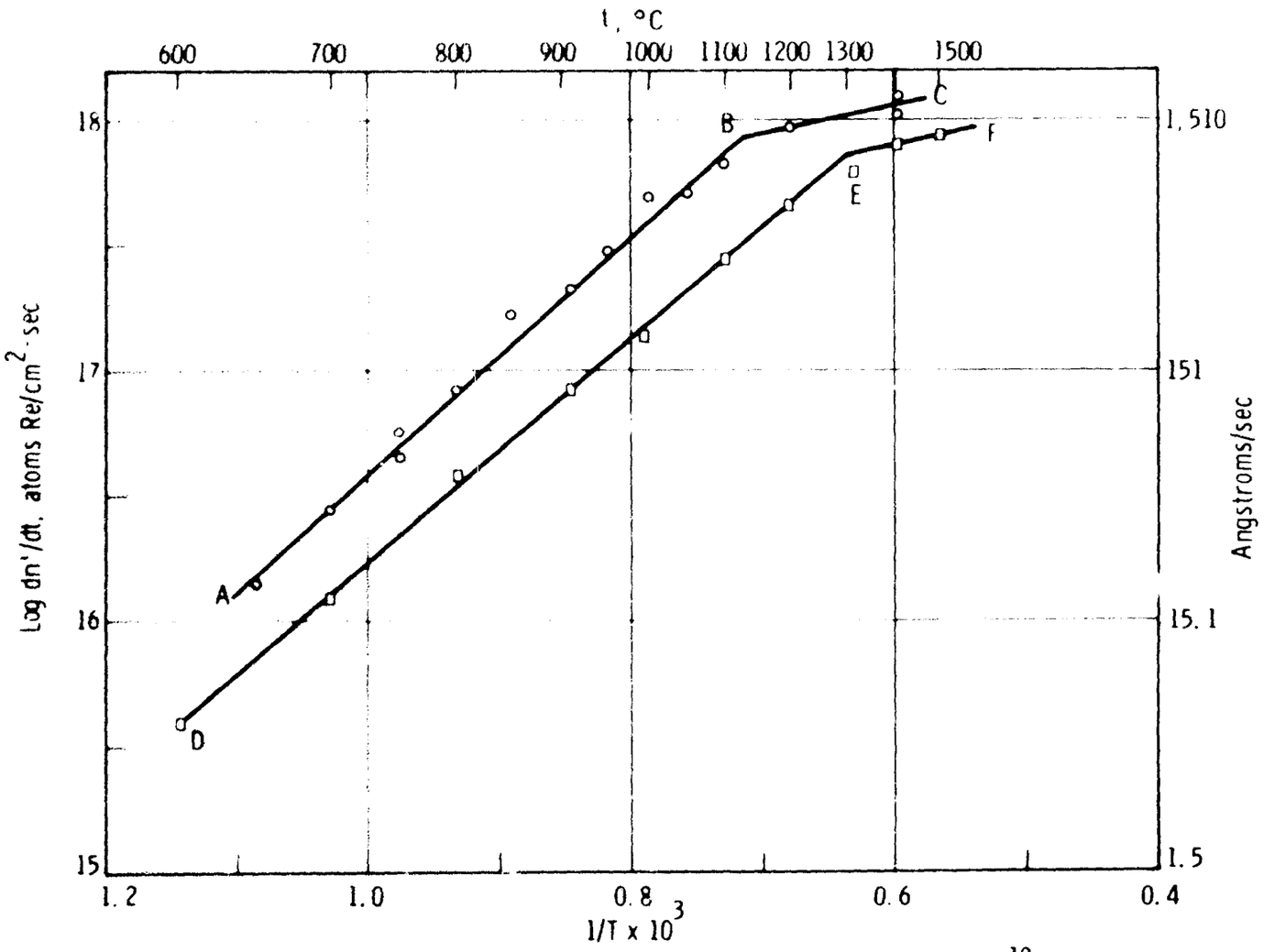

Fig. 1 – Log dn'/dt vs 1/T, oxidation Re-8% Ti, 600° - 1400°C, flow 0.28 - 1.97 × 10^{19} O_2 molecules/sec, ABC - 5 torr, DEF - 2 torr

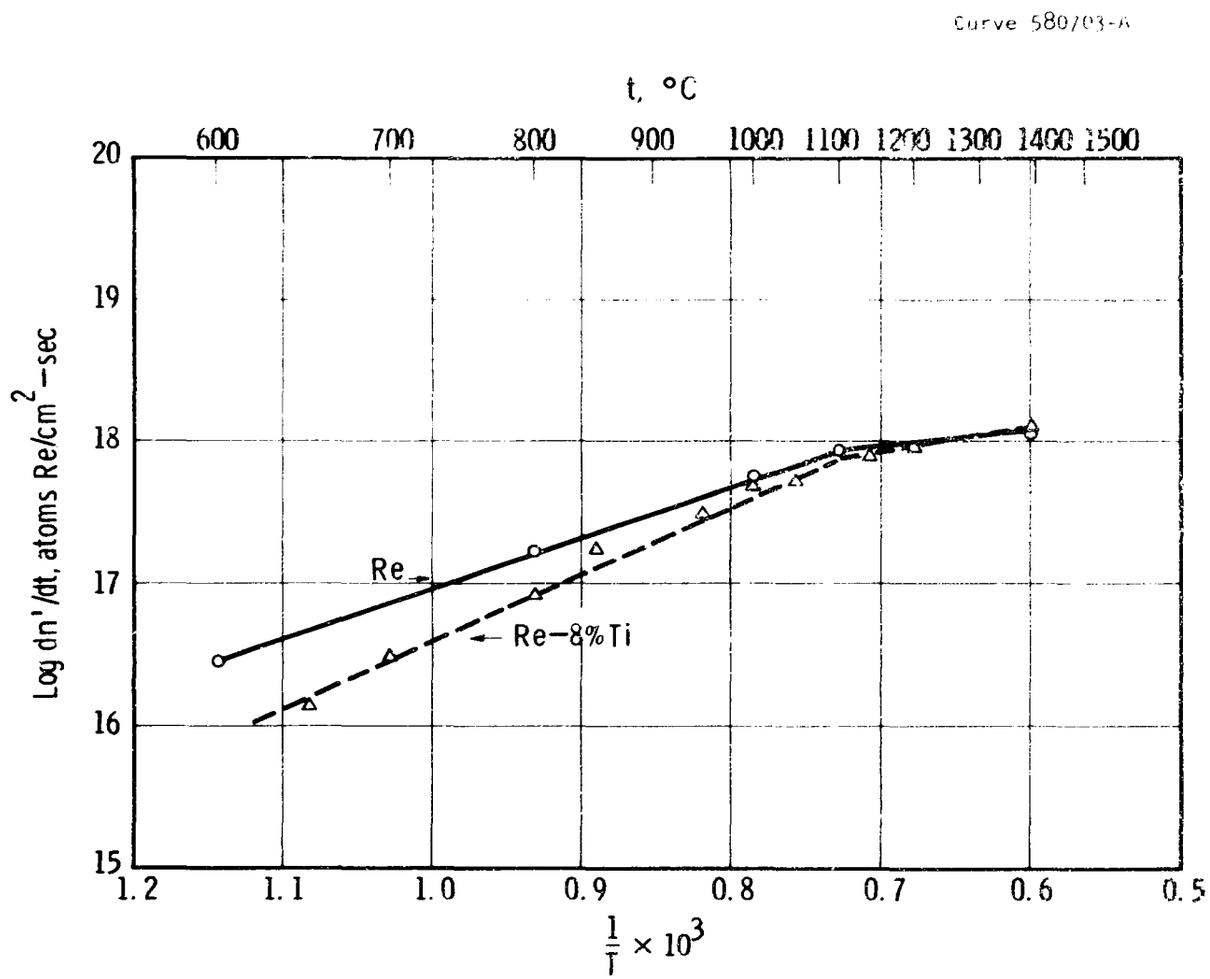

Fig. 8—Comparison high purity Re with Re—8%Ti alloy, log dn'/dt vs $\frac{1}{T}$, 5 torr

o——o Re, △- - -△ Re—8%Ti

Another probable chemical mechanism is desorption of the oxide. The activated state theory expression for desorption[12] is

$$dn'/dt + S/\ell \times C_a \, kT/h \times \exp(-\Delta H_2/RT) \qquad (2)$$

where C_a is the number of reaction sites per cm^2 and ΔH_2 is enthalpy of activation of desorption.

According to the activated state theory of surface reactions, zero order chemical surface reaction would give the same equation as that given for desorption. To apply these equations it is necessary to determine dn'/dt, ΔH, and the pressure dependence of dn'/dt.

Equation 1 for mobile adsorption of oxygen molecules can be fitted to the data of Figure 6 for 2, 5, and 10 torr oxygen pressures using $\Delta H = 16.8$ kcal/mole. Table 2 shows a comparison of the experimental rates of oxidation at 1000°C with values calculated from the mobile adsorption model and the desorption model of chemical processes. The agreement with the mobile adsorption model is good if a surface area of 1 or 2 for each cm^2 of geometrical area is used. The pressure dependence at 1000°C is $P^{0.57}$. Although the mobile adsorption equation fits the experimental data, a closer analysis of the pressure dependence indicates additional factors are affecting the rates of oxidation in addition to an adsorption process.

In Table 2 we assumed all of the gas was involved in mobile adsorption with an activation energy of 16.8 kcal for pure rhenium. Actually we postulate a monolayer of oxygen is preliminarily adsorbed with a lower activation energy and that mobile adsorption of oxygen occurs on this surface. This adsorption complex undergoes chemical reaction and desorption to form Re_2O_7.

---

12. S. Glasstone, K. J. Laidler and H. Eyring, Theory of Rate Processes, McGraw Hill Book Co., New York (1941).

Table 2

Comparison Theoretical and Experimental Rates of Oxidation at 1000°C
2 and 5 Torr Oxygen Pressure

Reaction Conditions		Rates of Oxidation (atoms/cm^2-sec)		
Pressure Torr	Flow Molecules/sec	Experimental	Theory Adsorption*	Theory Desorption
A. Rhenium				
2	4.81×10^{18}	3.08×10^{17}	2.66×10^{17}	2.0×10^{25}
5	1.84×10^{19}	5.53×10^{17}	6.64×10^{17}	2.0×10^{25}
B. Re-8% Ti				
2	3.1×10^{18}	0.74×10^{17}	0.48×10^{17}	1.1×10^{25}
5	1.77×10^{19}	1.9×10^{17}	1.24×10^{17}	1.1×10^{25}

*Stoichiometric factor used = 1.75

We conclude that the mechanism of oxidation of rhenium for the region AB of Figure 6 is probably mobile adsorption of oxygen modified by thickness or structural changes at the reaction interface. Studies of the reaction interface would be necessary to establish a complete mechanism.

2.5.2 Flow and Kinetic Theory Efficiencies

The flow efficiency, E, is given by the equation

$$E = dn/dt \times \ell \times 1/F \times 100 \qquad (3)$$

where F is the flow in oxygen molecules per second and dn/dt is the rate of reaction in atoms of Re/sec. The percent of oxygen molecules passing over the sample which react is given by E.

The kinetic theory efficiency, ε, is given by

$$\varepsilon = dn'/dt \times \ell \times 1/n \times 100 \qquad (4)$$

where n is the number of oxygen molecule collisions with a cm^2 of surface. n is given by the equation

$$n = 3.5 \times 10^{22} \times P/(MT)^{1/2} \qquad (5)$$

where P is the pressure in torr, T is the temperature and M the molecular weight. The kinetic theory efficiency gives the fraction of total collisions which react.

Table 3 gives both the flow and kinetic theory efficiencies in the gas diffusion region of reaction.

Table 3

Flow and Kinetic Theory Efficiency Calculations

Reaction Conditions			Efficiencies	
Temp. °C	Pressure Torr	Flow O_2 molecules/sec.	Flow E %	Kinetic Theory ε %
A. Rhenium				
1400	1	1.39×10^{19}	7.6	0.88
1400	2	4.98×10^{18}	18.6	0.40
1400	5	1.85×10^{19}	6.3	0.24
1400	10	1.91×10^{19}	6.6	0.14
B. Re-8% Ti				
1507	2	3.6×10^{18}	25.4	0.51
1400	5	1.7×10^{19}	6.9	0.25

3. OXIDATION OF MOLYBDENUM IN FLOW ENVIRONMENTS AT TEMPERATURES OF 900° TO 1600°C AND AT OXYGEN PRESSURES OF 9×10^{-3} TO 49 TORR

3.1 Introduction

The oxidation of molybdenum from room temperature to 1700°C involves a number of different oxidation processes.[2] Below 600°C a compact oxide film is formed which acts to prevent further reaction. The oxide film begins to volatilize at 600°C. At 795°C the oxide melts. Above 800°C oxidation occurs without appreciable oxide film formation. The volatile oxides consist of polymers of MoO_3. Chemical processes on the metal interface are rate controlling. Above a certain transition temperature, the primary chemical reactions are masked by gas diffusion of oxygen through a barrier layer of reaction products to the gas-metal interface for reaction. This transition temperature depends on the pressure, specimen size, gas flow, and the reaction system.

This paper will present new studies on the high temperature oxidation of molybdenum using a flow reaction system for a number of pressures over the temperature range of 900° to 1600°C. The purpose of the study is to investigate the reaction conditions under which chemical processes are rate controlling. The influence of gas flow and of pressure are of special interest.

3.2 Experimental

The reaction system differs in some details from that used in earlier studies.[1][2] Larger diameter stainless steel tubing was used to connect the furnace tube and balance housing. This arrangement

facilitated the measurement of the pressure at low pressure when large fractions of the oxygen gas were consumed by the reaction. The molybdenum specimen was suspended from one end of a Cahn electrobalance[13] enclosed in the reaction system. Oxygen was preheated and passed over the specimen. An auxiliary fore pump was used to pump the oxygen gas through the system. For the low pressure runs, the mercury vapor diffusion pumps were used to pump the oxygen gas over the sample.

The flow rate and gas pressure were maintained constant by a sensitive leak valve. The volume and flow rate of the oxygen used were calculated from measurements of the pressure change of a calibrated gas-reservoir. The system pressure and flow rate were changed by controlling the exit pumping speed and the volume of gas added through the leak valve.

The Cahn balance had a capacity of about 1 g, a sensitivity of better than 10^{-6} g for a 1 g sample and a period of less than 0.1 sec. To support the sample, a section of 8 mil Pt wire was used in the hot zone and a section of 2 mil nickel-chromium wire was used in the cold zone.

The furnace tube, balance housing and associated apparatus were attached to a series of mercury diffusion pumps and a fore pump. A liquid-nitrogen trap was used to condense the mercury vapor. At 1200°C a vacuum of lower than 2×10^{-6} torr could readily be achieved.

A Kanthal-Super furnace was used. Its construction and operation has been described.[7] The temperature of the specimen was determined by a Pt-Pt + 10% Rh thermocouple mounted adjacent to the specimen inside the furnace tube. The thermocouple was calibrated to 1200°C. Maximum temperature variation of the furnace was $\pm$ 5°C.

Precision Wallace-Tiernan pressure gauges were used to measure pressures above 1 torr. Calibrated thermocouple gauges were used to

---

13. L. Cahn, Instruments and Control Systems 35, 107 (1962).

measure pressures from 5×10^{-3} to 0.5 torr. The thermocouple gauges were attached directly to the furnace tube to measure the pressure in the reaction zone.

Specimens were machined from high purity molybdenum rod and polished through 4/0 polishing paper. Samples were then cleaned in petroleum ether and alcohol. The standard specimen was a cylinder with hemispherical ends, 0.16 cm in diameter, 1.2 cm long, 0.6 cm^2 surface area and weighing 0.24 g.

Spectroscopic analysis showed the following impurities in parts per million: Cu 10, Cr 45, Mn 5, Al 40, Fe 200, Ca 10, Ni 70, Sn 10, Mg 5, Si 50, and B 1. The elements Ba, Sr, Pb, Co, Ag, Cd, V, Nb and Ti were not detected.

Commercial grade oxygen and air were used. The gases were dried before using.

3.3 Method

The specimens were suspended from the balance, the system closed and then evacuated to a pressure of 2×10^{-6} torr. The furnace was raised about the furnace tube and the vacuum read on an ion gauge or a McLeod gauge. After the desired reaction temperature was reached, oxygen was added directly from the reservoir to avoid having the gas come in contact with mercury. The auxiliary pump or mercury pumping system was used to exhaust the gases. A liquid-nitrogen trap was placed between the reaction system and mercury pumps to minimize mercury contamination.

Weight changes of the molybdenum specimen and pressure changes of the oxygen reservoir were read and recorded as a function of time. The oxygen pressure in the reaction system was maintained constant. Readings were made at 15 sec intervals. Continuous adjustment of the leak valve was necessary to maintain constant pressure and reproducible balance readings.

3.4 Results

The oxidation of molybdenum was studied at temperatures from 900°C to 1600°C in oxygen at 9×10^{-3}, 4×10^{-2}, 1×10^{-1}, 2, 19, and 49 torr. The oxygen flow rates were 0.7×10^{17} to 8.5×10^{19} molecules oxygen per second.

The flow rate of oxygen through the furnace tube is calculated from the pressure change of the calibrated gas-reservoir in units of molecules of oxygen per sec. This value is then converted to atoms of oxygen per second, which permits a direct calculation of the efficiency of the oxidation processes.

The rates of oxidation were determined from the nearly linear weight-loss versus time plots of the data. The rate, dw/dt, in g/sec was determined at time t = 0 before surface area changes occur. Avogadro's number is used to convert the oxidation rate, dw/dt, to atoms of Mo reacting per sec, dn/dt. To compare the oxidation rates with theoretical predictions, the oxidation rate is given in units of atoms of molybdenum reacting per cm^2, dn'/dt. The velocity of the gases over the specimen can be calculated from the flow rate and the cross sectional area, 3.14 cm^2, of the tube.

Table 4 summarizes the kinetic studies. The reaction conditions are given at the left and the rates of oxidation at the right. The kinetic data are given in both weight units and in atoms of molybdenum reacting per cm^2-sec. Surface temperatures were estimated as described in an earlier paper.[14]

Figure 9 shows a summary of the kinetic data. The logarithm of the rate of oxidation in atoms of Mo per cm^2-sec is plotted against 1/T. The data are compared to results on molybdenum oxidation at 76 torr obtained using a static reaction system and specimens of

---

14. E. A. Gulbransen, K. F. Andrew and F. A. Brassart, Carbon 1, 413 (1964).

Table 4

Summary Kinetic Data Oxidation of Molybdenum 900°-1600°C in Flow Environments at Oxygen Pressures of 9×10^{-3} to 49 Torr

Reaction Conditions				Rates of Reaction			
Pressure (torr)	Furnace Temp. °C	Surface Temp. °C Estimated	Flow (atoms O/sec)	dw/dt (g/sec)	dn/dt (atoms/sec)	dn'/dt (atoms/cm^2-sec)	log dn'/dt
9×10^{-3}	1000	1000	2.9×10^{17}	1.04×10^{-7}	6.5×10^{14}	1.09×10^{15}	15.036
	1100	1100	2.9×10^{17}	3.0×10^{-7}	1.86×10^{15}	3.1×10^{15}	15.492
	1200	1200	2.9×10^{17}	8.6×10^{-7}	5.4×10^{15}	9.0×10^{15}	15.954
	1300	1300	2.9×10^{17}	2.4×10^{-6}	1.5×10^{16}	2.46×10^{16}	16.391
	1400	1400	2.9×10^{17}	5.5×10^{-6}	3.5×10^{16}	5.7×10^{16}	16.757
	1600	1600	2.9×10^{17}	1.4×10^{-5}	8.7×10^{16}	1.43×10^{17}	17.155
4×10^{-2}	1000	1000	1.4×10^{17}	8.6×10^{-7}	5.4×10^{15}	8.9×10^{15}	15.951
	1100	1100	1.4×10^{17}	1.25×10^{-6}	7.8×10^{15}	1.29×10^{16}	16.112
	1200	1200	1.4×10^{17}	2.26×10^{-6}	1.42×10^{16}	2.34×10^{16}	16.369
	1300	1300	2.9×10^{17}	6.5×10^{-6}	4.06×10^{16}	6.7×10^{16}	16.827
	1500	1502	5.8×10^{17}	2.5×10^{-5}	1.57×10^{17}	2.60×10^{17}	17.414
1×10^{-1}	900	900	6.7×10^{17}	8.3×10^{-7}	5.2×10^{15}	8.7×10^{15}	15.937
	900	900	6.7×10^{17}	5.3×10^{-7}	3.4×10^{15}	5.6×10^{15}	15.745
	1000	1000	6.7×10^{17}	1.63×10^{-6}	1.02×10^{16}	1.70×10^{16}	16.23
	1100	1100	6.7×10^{17}	3.9×10^{-6}	2.45×10^{16}	4.0×10^{16}	16.609
	1200	1200	6.7×10^{17}	8.2×10^{-6}	5.2×10^{16}	8.6×10^{16}	16.933
	1400	1426	1.35×10^{18}	3.4×10^{-5}	2.1×10^{17}	3.5×10^{17}	17.547
	1600	1612	2.2×10^{18}	8.1×10^{-5}	5.1×10^{17}	8.4×10^{17}	17.923

(Continued)

Table 4 (Continued)

Reaction Conditions				Rates of Reaction			
Pressure (torr)	Furnace Temp. °C	Surface Temp. °C Estimated	Flow (atoms O/sec)	dw/dt (g/sec)	dn/dt (atoms/sec)	dn'/dt (atoms/cm^2-sec)	log dn'/dt
2	900	900	5.4×10^{18}	3.0×10^{-6}	1.9×10^{16}	3.2×10^{16}	16.50
	1000	1004	5.4×10^{18}	8.8×10^{-6}	5.5×10^{16}	9.1×10^{16}	16.96
	1100	1104	5.4×10^{18}	1.8×10^{-5}	1.1×10^{17}	1.83×10^{17}	17.26
	1200	1207	5.4×10^{18}	2.6×10^{-5}	1.64×10^{17}	2.72×10^{17}	17.43
	1400	1410	5.4×10^{18}	5.5×10^{-5}	3.43×10^{17}	5.7×10^{17}	17.75
5	900	904	5.4×10^{18}	7.6×10^{-6}	4.8×10^{16}	7.9×10^{16}	16.90
	1000	1007	5.4×10^{18}	1.56×10^{-5}	9.8×10^{16}	1.63×10^{17}	17.21
	1200	1213	5.4×10^{18}	4.2×10^{-5}	2.6×10^{17}	4.34×10^{17}	17.64
	1400	1411	8.1×10^{18}	9.2×10^{-5}	5.8×10^{17}	9.64×10^{17}	17.98
19	900	909	2.7×10^{19}	1.54×10^{-5}	9.7×10^{16}	1.6×10^{17}	17.21
	1100	1123	2.7×10^{19}	6.9×10^{-5}	4.3×10^{17}	7.2×10^{17}	17.85
	1300	1339	2.8×10^{19}	1.33×10^{-4}	8.3×10^{17}	1.38×10^{18}	18.14
	1500	1528	3.2×10^{19}	1.89×10^{-4}	1.2×10^{18}	1.96×10^{18}	18.29
49	817	837	1.6×10^{20}	2.85×10^{-5}	1.8×10^{17}	3.0×10^{17}	17.477
	914	975	1.7×10^{20}	1.17×10^{-4}	7.4×10^{17}	1.24×10^{18}	18.093
	1010	1111	1.7×10^{20}	2.6×10^{-4}	1.63×10^{18}	2.74×10^{18}	18.44
76	1000						18.10

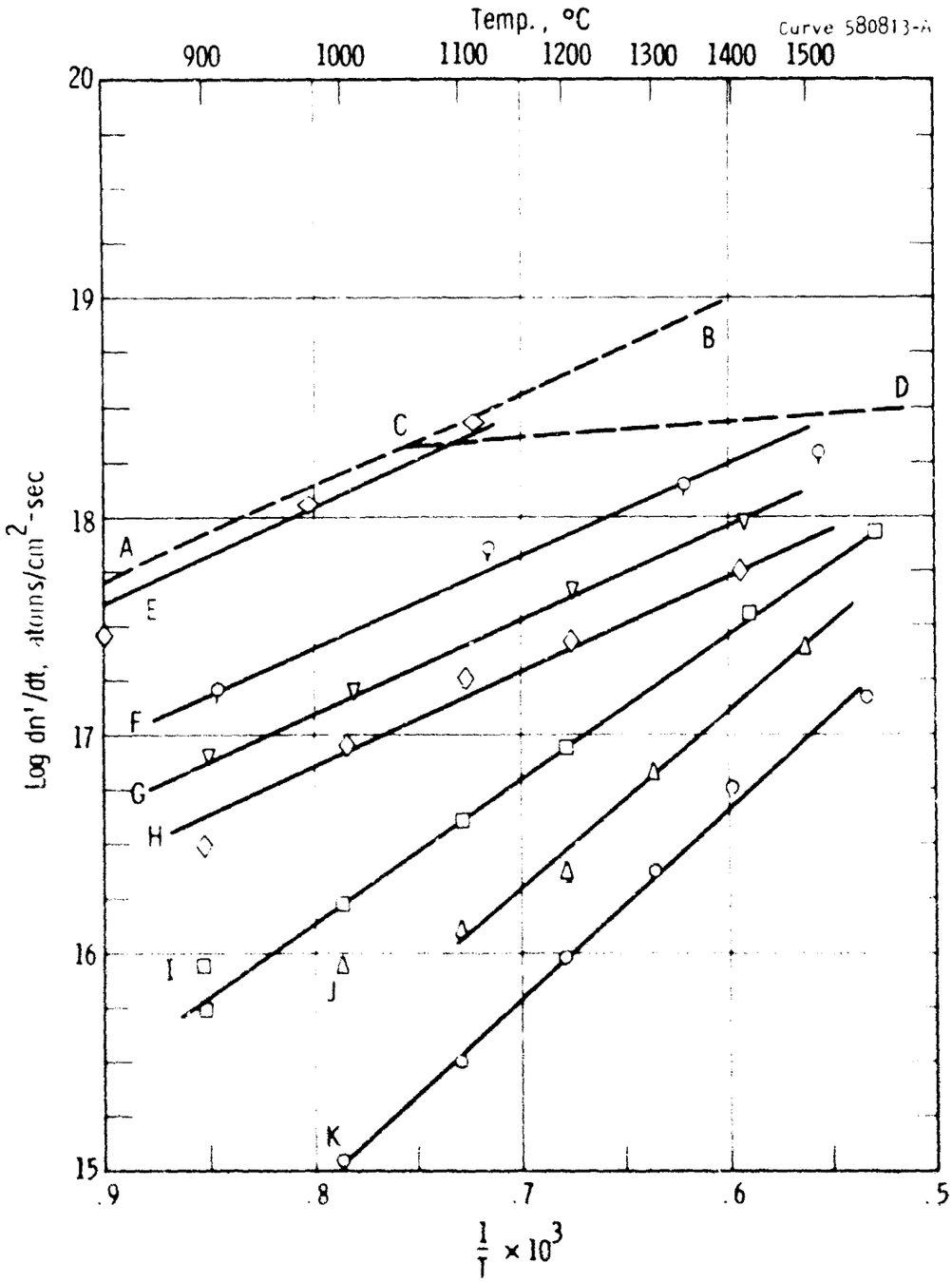

Fig. 9—Log dn'/dt vs 1/T, oxidation of molybdenum AB chemical control 76 torr O_2 pressure, ACD experimental results static system 0.6 cm^2 samples; E, F, G, H, I, J, K results flow system; E-49 torr, F-19 torr, G-5 torr, H-2 torr, I = 1×10^{-1} torr, J-4×10^{-2} torr, K-9×10^{-3} torr

0.6 cm^2 area.[2] For the chemical controlled oxidation region, these results are in good agreement with results obtained using the flow reaction system. The data fall on straight lines. A heat of activation of 41 kcal/mole was calculated for the 9×10^{-3} and 4×10^{-2} torr series of experiments while a heat of activation of 29 kcal/mole was found for the 1×10^{-1} torr series of experiments. A heat of activation of 19.7 kcal was found in an earlier work for a pressure of 76 torr. The heats of activation for the 2, 5, 19 and 49 torr series are in agreement with that found for the 76 torr series of experiments.

Figure 10 shows the effect of pressure on the rate of oxidation at four temperatures, 1000°, 1100°, 1200° and 1400°C. The pressure dependence varies from $P^{0.77}$ to $P^{0.7}$. This pressure dependence suggests that the reaction mechanism is complex.

3.5 Discussion of Mechanisms

3.5.1 Efficiency of Calculations

Two types of efficiencies are used to compare the experimental oxidation rates with kinetic theory and with the actual flow rate of oxygen molecules and atoms over the sample. The kinetic theory expression for the collision number n, is given by

$$n = 3.5 \times 10^{22} \times P/(MT)^{1/2} \qquad (6)$$

Here P is the pressure in torr, M is the molecular weight and T is the temperature. The kinetic theory efficiency ε, is given by

$$\varepsilon = dn'/dt \times \ell \times 1/n \times 100 \qquad (7)$$

Here ℓ is the stoichiometric factor, $\ell = 2/3$ for the formation of MoO_3.

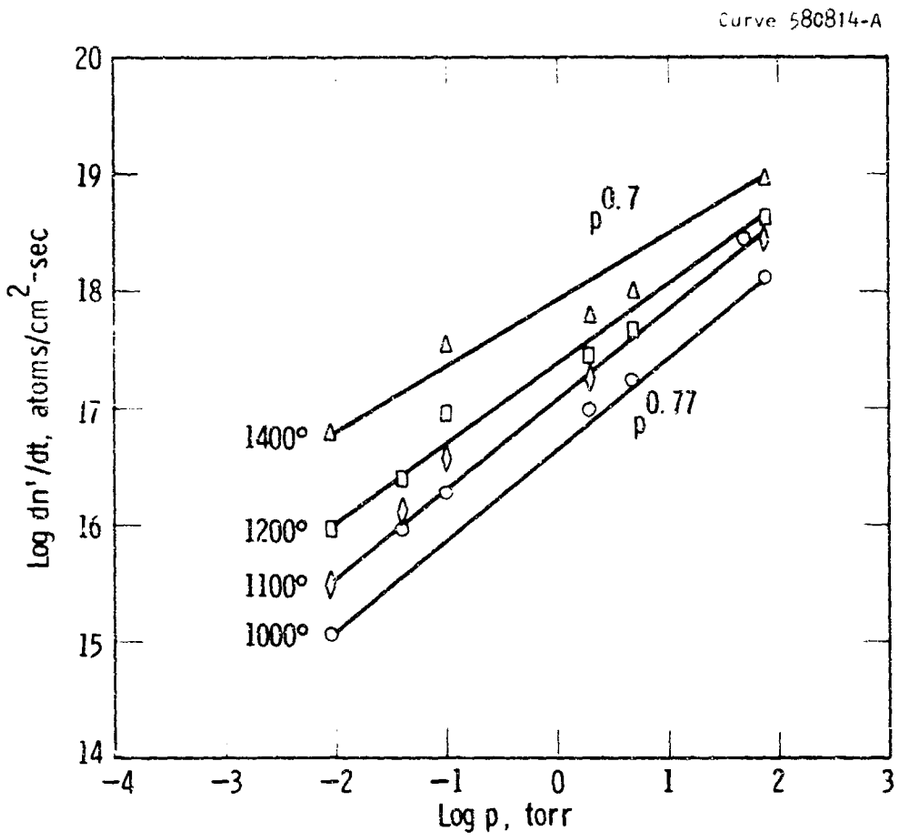

Fig. 10—Log rate vs log pressure, oxidation of molybdenum
○-1000°C, ◊-1100°C, □-1200°C, Δ-1400°C

The second efficiency compares the experimental rate of reaction with the rate of gas flowing over the sample. Flow efficiencies, E, are calculated from the equation

$$E = 3\ dn'/dt \times A \times 1/F \times 100 \qquad (8)$$

Here A is the surface area, F is the flow rate in atoms of O per sec, dn'/dt is the rate of reaction in terms of atoms of Mo per cm^2-sec and 3 is the stoichiometric ratio of O/Mo in MoO_3.

Table 5 shows a summary of the two efficiency calculations. The kinetic theory efficiencies reach a value of 0.166 at 1600°C and 9×10^{-3} torr pressure. Flow efficiencies up to 0.89 were calculated. Nearly all of the oxygen leaked into the reaction system is consumed by the molybdenum sample.

Table 5 shows the kinetic theory and flow efficiencies to be a function of temperature and of pressure. The two efficiencies increase with temperature and decrease with pressure.

Rosner and Allendorf[15] have also observed high efficiencies for the molybdenum-oxygen reaction. They found a heat of activation of 26 kcal per mole for the reaction of molecular oxygen with molybdenum. Complex departures from first order kinetics were observed. Oxygen atoms were found to be more reactive than O_2 molecules. At 1200°K the efficiencies of reaction for O atoms was 100 times higher than for O_2 molecules. One Mo atom was reacted for every ten O atoms striking a 1200°K surface.

We have not studied the O atom reaction directly; however at low pressure appreciable concentrations of O atoms exist in equilibrium with oxygen molecules. At 1600°C and 9×10^{-3} torr oxygen pressure an

---

15. D. E. Rosner and H. D. Allendorf, J. Chem. Phys. 40, 3441 (1964).

Table 5

Kinetic Theory and Flow Efficiencies

Reaction Conditions			Rate of Oxidation	Efficiencies	
Temp. °C	Pressure Torr	Flow Atoms O/sec	dn'/dt Atoms Mo/cm^2-sec	Kinetic Theory %	Flow %
1000	9×10^{-3}	2.9×10^{17}	1.09×10^{15}	0.11	0.68
1100	9×10^{-3}	2.9×10^{17}	3.1×10^{15}	0.31	1.92
1200	9×10^{-3}	2.9×10^{17}	9.0×10^{15}	0.93	5.6
1300	9×10^{-3}	2.9×10^{17}	2.5×10^{16}	2.66	15.6
1400	9×10^{-3}	2.9×10^{17}	5.7×10^{16}	6.24	35.4
1600	9×10^{-3}	2.9×10^{17}	1.43×10^{17}	16.6	89.0
1000	4×10^{-2}	1.4×10^{17}	8.93×10^{15}	0.19	11.0
1100	4×10^{-2}	1.4×10^{17}	1.29×10^{16}	0.29	16.1
1200	4×10^{-2}	1.4×10^{17}	2.34×10^{16}	0.55	29.2
1300	4×10^{-2}	2.9×10^{17}	6.71×10^{16}	1.60	41.7
1500	4×10^{-2}	5.8×10^{17}	2.60×10^{17}	6.60	80.6
900	1×10^{-1}	6.7×10^{17}	8.70×10^{15}	0.07	2.3
0	1×10^{-1}	6.7×10^{17}	1.70×10^{16}	0.15	4.6
1100	1×10^{-1}	6.7×10^{17}	4.1×10^{16}	0.37	11.0
1200	1×10^{-1}	6.7×10^{17}	8.6×10^{16}	0.80	23.0
1400	1×10^{-1}	1.4×10^{18}	3.5×10^{17}	3.5	45.0
1600	1×10^{-1}	2.2×10^{18}	8.4×10^{17}	8.8	69.0
1400	2	5.4×10^{18}	5.7×10^{17}	0.28	19.1
1400	5	8.1×10^{18}	9.64×10^{17}	0.19	21.5

O atom pressure of 6.3×10^{-4} torr was calculated.[16] The ratio of P_O to P_{O_2} is 7 percent. Assuming three O atoms are required to remove one Mo atom, the collision rate of the O atoms is not sufficient to account for more than 30% of the observed reaction. Similar calculations at 1300°C show that 8 percent of the rate of oxidation can be due to O atoms. At 1000°C only 1.9 percent of the experimental rate of oxidation can be due to O atoms.

Although O atoms due to thermal dissociation were present in the reacting gas, the calculated collision rates were not sufficient to account for the high rates of reaction that were observed experimentally.

3.5.2 Absolute Reaction Rate Theory

In an earlier paper we applied the predictions of the absolute reaction rate theory with the experimental rate of oxidation of molybdenum at 900°C and 76 torr oxygen pressure.[2] The calculations were based on an experimental heat of activation 19.7 kcal/mole. Mobile adsorption of oxygen molecules was shown to be the most feasible mechanism for the oxidation of molybdenum. The molybdenum surface was assumed to be covered with a surface layer of oxygen. The equations for the mobile adsorption and desorption mechanisms of reaction were given in an earlier section of this report. (2.5.1)

Table 6 shows the results obtained in this study together with those of the earlier study using the static type of reaction system and a pressure of 76 torr. The comparison is made for the chemical controlled region of oxidation. Again the mobile adsorption mechanism gives the best fit to the experimental data.

---

16. JANAF Thermochemical Tables, The Dow Chemical Co., Midland, Michigan.

Table 6

Correlation of Absolute Reaction Rate Theory with Experimental Rates of Oxidation of Molybdenum 900° and 1000°C

ΔH = 19.7 kcal/g mole

Reaction Conditions			Rates of Oxidation dn'/dt (atoms/cm^2-sec)		
Temp. °C	Pressure Torr	Flow Molecules O_2/sec	Experimental	Theory	
				Adsorption	Desorption
900	76	--	1.08×10^{18}	3.6×10^{17}	1.29×10^{24}
1000	49	8.5×10^{19}	2.74×10^{18}	5.3×10^{18}	2.2×10^{25}
1000	5	2.7×10^{18}	1.63×10^{17}	5.5×10^{18}	2.2×10^{25}
1000	2	2.7×10^{18}	9.1×10^{16}	2.2×10^{17}	2.2×10^{25}
1000	9×10^{-3} ‡	1.45×10^{17}	1.09×10^{15}	2.1×10^{11}	4.83×10^{20}

‡Calculated on basis of ΔH = 41 kcal/g mole.

Calculations for the results at 9×10^{-3} torr and 4×10^{-2} torr, where a heat of activation of 41 kcal/mole was obtained, cannot be interpreted by either an adsorption or desorption mechanism for reaction. These calculations are also shown in Table 6. Mobile adsorption gives a rate too slow to explain the rate of reaction, while the desorption calculation is too fast. This region of reaction will require further experimentation.

4. THERMOCHEMICAL ANALYSES ON THE OXIDATION OF MOLYBDENUM

The thermochemical conditions during the oxidation of molybdenum are complex since several oxides are formed. In addition, the oxides can exist as solids, liquids and gases.

Table 7 shows the several oxidation and volatilization reactions which occur in the oxidation of molybdenum. The expressions for the equilibrium constant and the values of the logarithm of the equilibrium constants for temperatures between 1000° and 2000°K are tabulated for each of the reactions.

The thermochemical data for MoO(g), MoO_2(s), MoO_2(g), MoO_3(s), MoO_3(g), and Mo(g) are taken from the JANAF Tables.[16] The thermochemical data for $(MoO_3)_n$(g) where n is about 3 was taken from a paper by Gulbransen, Andrew and Brassart.[17]

Figures 11 to 14 show a graphical interpretation. In these figures the logarithm of the volatile oxide pressure in atmospheres is plotted against the logarithm of the oxygen pressure in atmospheres. Vertical lines represent dissociation pressures of the solid and liquid oxide phases. Horizontal lines represent volatility curves which are independent of oxygen pressure. The remaining curves represent the effect of oxygen pressure on the volatile oxide pressure for the given reaction. Lines to the left of MoO_2(s) in the figures relate to equilibria of the type

$$Mo(s) + O_2(g) \rightleftharpoons MoO_2(g) \qquad (9)$$

---

17. E. A. Gulbransen, K. F. Andrew and F. A. Brassart, J. Electrochem. Soc. 110, 242 (1963).

Table 7

Molybdenum Oxides, Equations for Formation, Equilibrium Constants and Values of Log K_p for Various Temperatures 1000° to 2000°K JANAF THERMOCHEMICAL TABLES

Reaction	Equilibrium Expression	log K_p at °K					
		1000	1200	1400	1600	1800	2000
1. $Mo(s) + 1/2\ O_2 \rightleftharpoons MoO(g)$	$K = p_{MoO}/(p_{O_2})^{1/2}$	-14.21	-11.08	-8.86	-7.20	-5.92	-4.91
2. $Mo(s) + O_2 \rightleftharpoons MoO_2(s)$	$K = 1/p_{O_2}$	21.24	16.21	12.64	9.98	7.94	6.35
3. $Mo(s) + O_2 \rightleftharpoons MoO_2(g)$	$K = p_{MoO_2}/p_{O_2}$	1.63	1.58	1.54	1.49	1.45	1.40
4. $Mo(s) + 3/2\ O_2 \rightleftharpoons MoO_3(s,1)$	$K = 1/(p_{O_2})^{3/2}$	25.81	19.72	15.54	12.40*	10.0*	8.0*
5. $Mo(s) + 3/2\ O_2 \rightleftharpoons MoO_3(g)$	$K = p_{MoO_3}/(p_{O_2})^{3/2}$	14.65	11.70	9.58	7.99	6.75	5.75
6. $MoO_2(s) + 1/2\ O_2 \rightleftharpoons MoO_3(s)$	$K = 1/(p_{O_2})^{1/2}$	4.57	3.51	--	--	--	--
7. $MoO_2(s) + 1/2\ O_2 \rightleftharpoons MoO_3(g)$	$K = p_{MoO_3}/(p_{O_2})^{1/2}$	-6.59	-4.51	-3.06	-1.99	-1.19	-0.60
8. $MoO_2(s) \rightleftharpoons MoO_2(g)$	$K = p_{MoO_2}$	-19.61	-14.63	-11.11	-8.494	-6.49	-4.95
9. $MoO_3(s) \rightleftharpoons MoO_3(g)$	$K = p_{MoO_3}$	-11.16	-8.02	-5.96	-4.41	--	--
10. $Mo(s) \rightleftharpoons Mo(g)$	$K = p_{Mo}$	-26.69	-20.97	-16.89	-13.85	-11.48	-9.60
11. $Mo(s) + 3/2\ O_2 \rightleftharpoons 1/3\ (MoO_3)_3(g)$	$K = (p_{(MoO_3)_3})^{1/3}/(p_{O_2})^{3/2}$	24.85	19.38	15.50	12.50	--	--
12. $MoO_3(s,1) \rightleftharpoons 1/3\ (MoO_3)_3(g)$	$K = p_{(MoO_3)_3}^{1/3}$	-0.955	-0.3446	-0.0393	+0.1646	-0.3676	+0.510

*Extrapolated

The equilibrium constant involves both $MoO_2(g)$ and $O_2(g)$. The $p_{MoO_2(g)}$ decreases as the p_{O_2} decreases. Lines to the right of $MoO_3(s,l)$ represent reactions of the type

$$MoO_3(s,l) \rightleftharpoons MoO_2(g) + 1/2\ O_2 \qquad (10)$$

Here the $p_{MoO_2(g)}$ remains constant or decreases as log p_{O_2} increases. The lines in the chart between $MoO_2(s)$ and $MoO_3(s,l)$ represent equilibria of the type

$$MoO_2(s) \rightleftharpoons MoO_2(g) \qquad (11)$$

Figures 11 to 14 can be used to predict the surface oxides formed on molybdenum during oxidation and the nature of the volatile species for a wide variety of oxidation conditions. At 1000°K, Figure 11, $MoO_2(s)$ and $MoO_3(s)$ should form with $MoO_2(s)$ next to the metal and $MoO_3(s)$ adjacent to the gas phase for oxygen pressures > log p_{O_2} = 9.4, i.e. $p_{O_2} = 3.98 : 10^{-10}$ atm. Between log p_{O_2} = -21.2 and -9.4, $MoO_2(s)$ would be found on the metal surface. $(MoO_3)_3(g)$ and $MoO_3(g)$ would be the volatile gases formed. The equilibrium pressures can be taken from Figure 11. For log p_{O_2} = -9.4, log $p_{MoO_3(g)}$ = -2.9.

Figure 12 shows the data at 1200°K. Above log p_{O_2} = -7.0, $MoO_3(l)$ and $MoO_2(s)$ are formed. Between log p_{O_2} = -16.2 and -7.0, $MoO_2(s)$ is formed. $(MoO_3)_3(g)$ and $MoO_3(g)$ are the volatile species. Below log p_{O_2} = -16.2 molybdenum oxidizes without oxide film formation to form $MoO_3(g)$ and $MoO_2(g)$ depending on log p_{O_2}. For log p_{O_2} < -22.6 molybdenum vaporizes.

Figure 13 shows the data at 1400°K. Above log p_{O_2} = -5.8 $MoO_3(l)$ and $MoO_2(s)$ are formed and $(MoO_3)_3$ is the volatile specie. Between log p_{O_2} = -12.6 and -5.8, $MoO_2(s)$ is formed. $(MoO_3)_3(g)$ and $MoO_3(g)$ are the volatile species. Below log p_{O_2} = -12.6 molybdenum oxidizes directly to $MoO_3(g)$ and $MoO_2(g)$ depending on log p_{O_2}. At log p_{O_2} < -18.4 Mo(g) is formed.

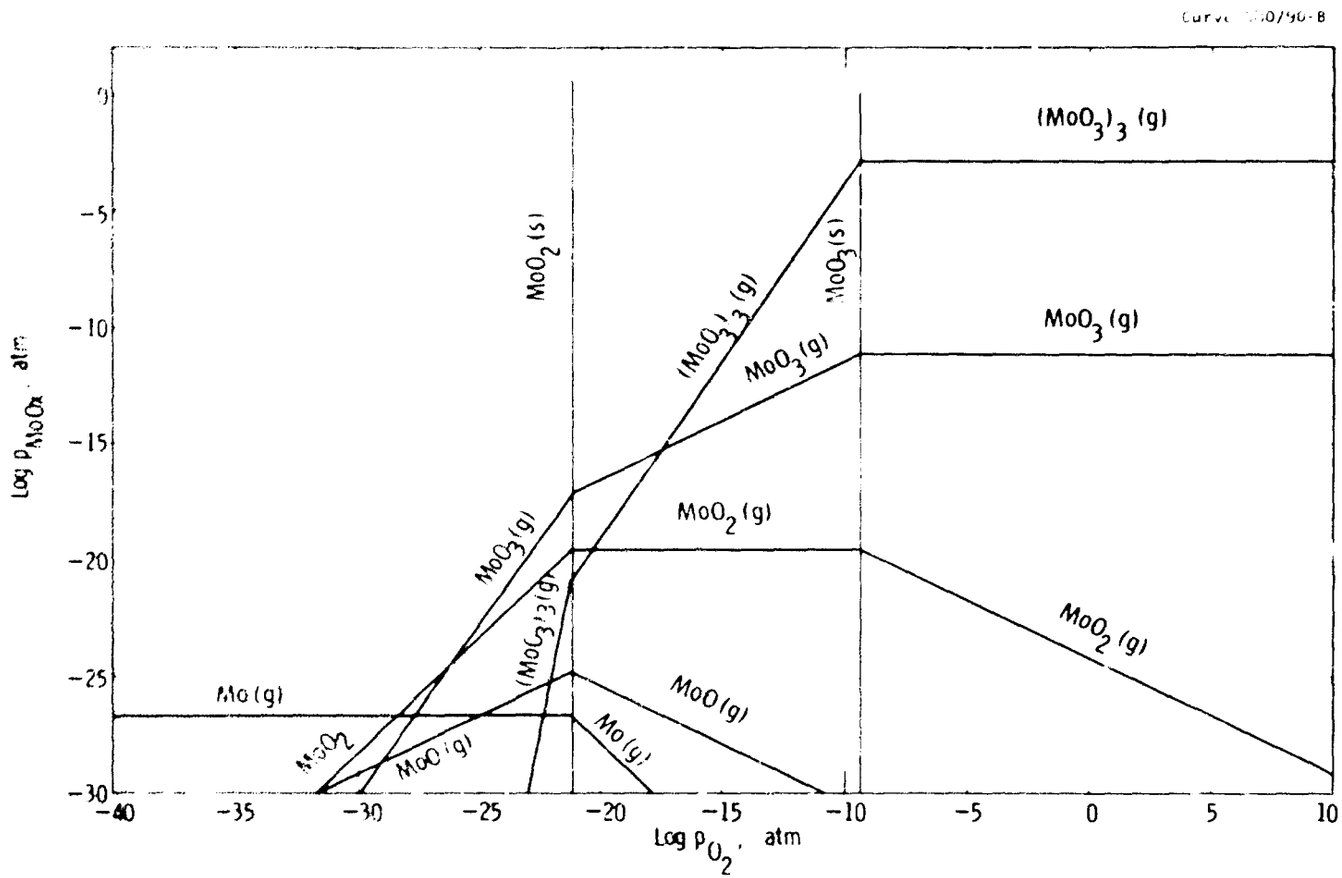

Fig. 11—Thermochemical data - oxidation of molybdenum, 1000°K

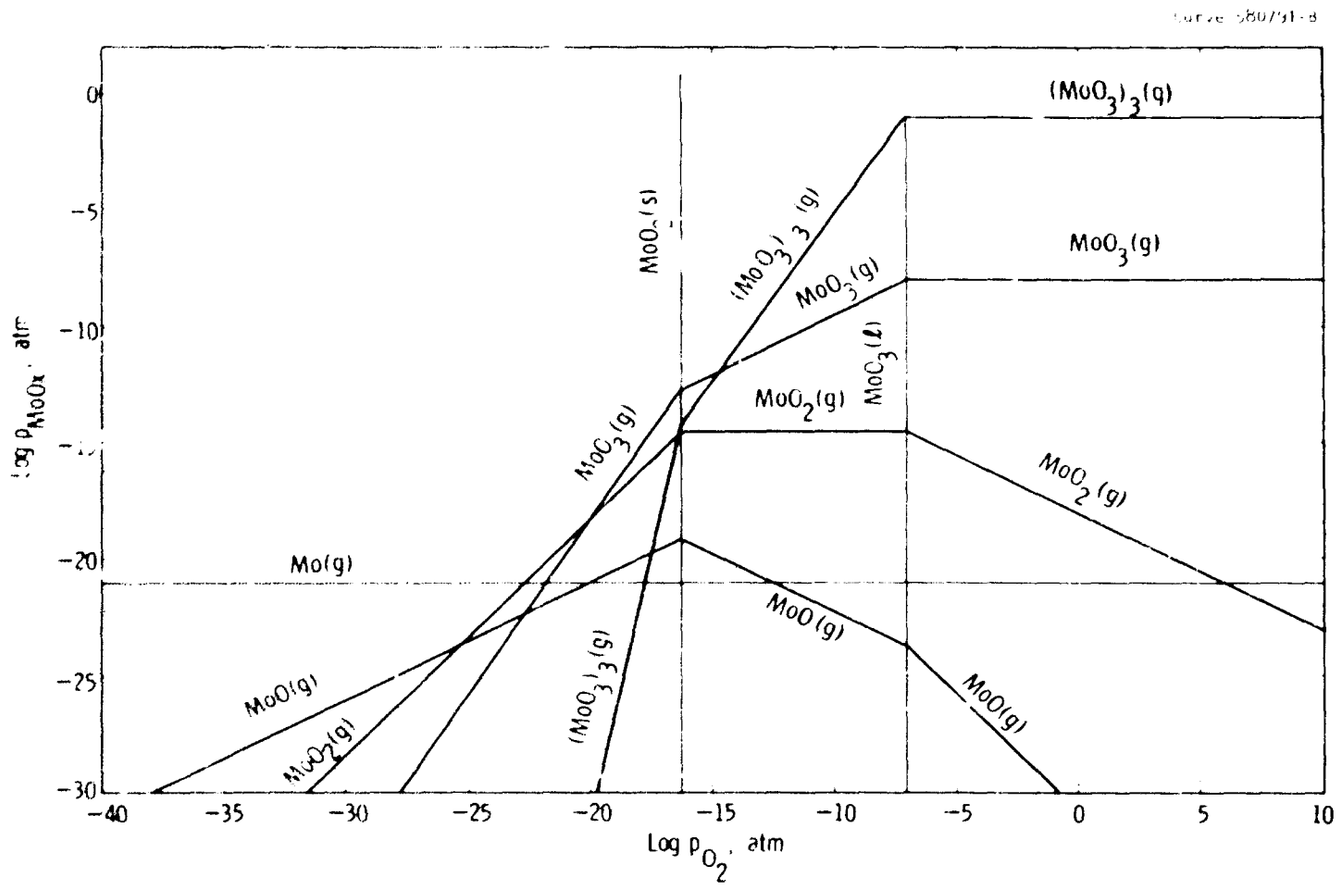

Fig. 12—Thermochemical data—oxidation of molybdenum, 1200°K

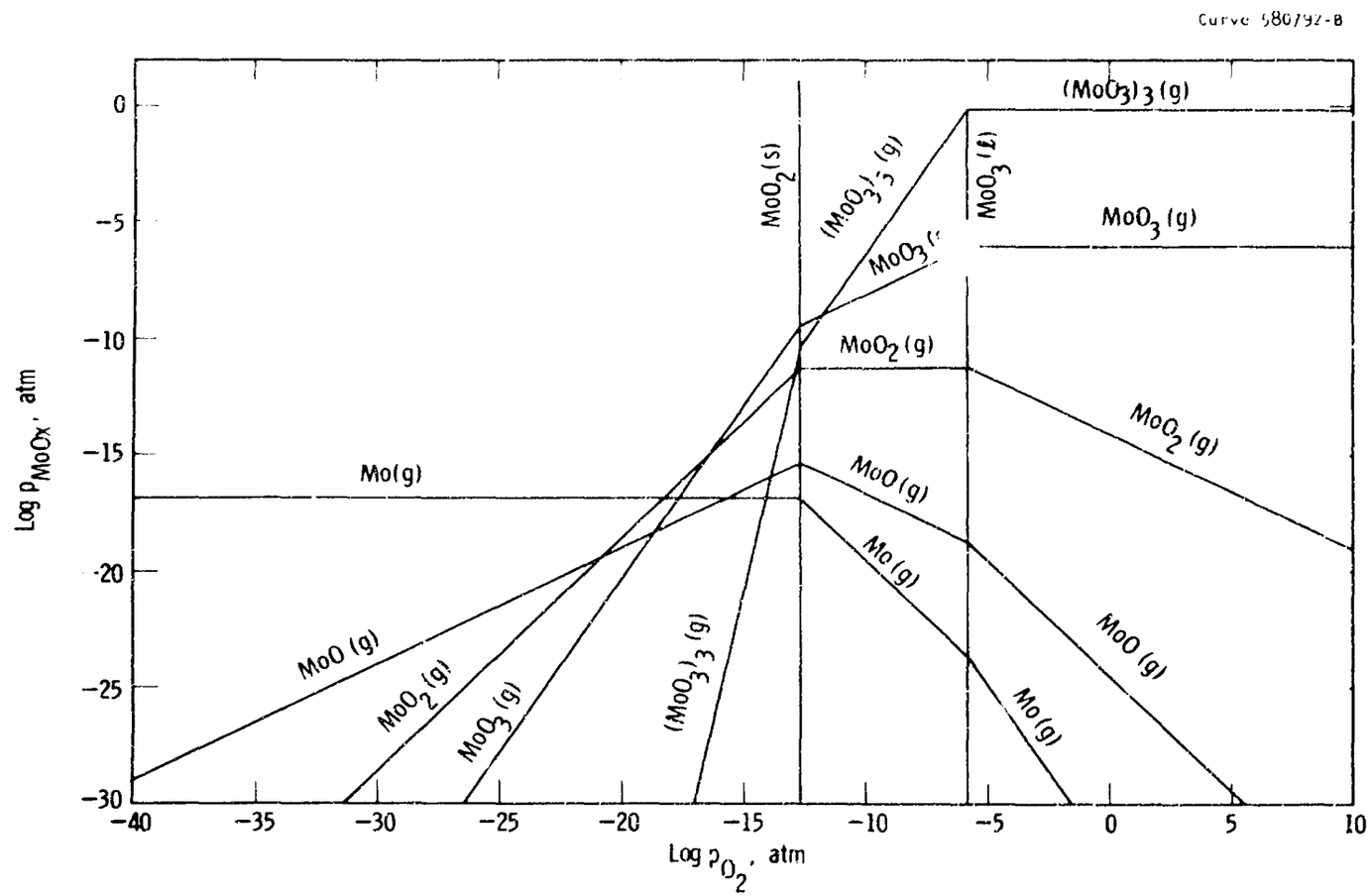

Fig. 13—Thermochemical data - oxidation of molybdenum, 1400°K

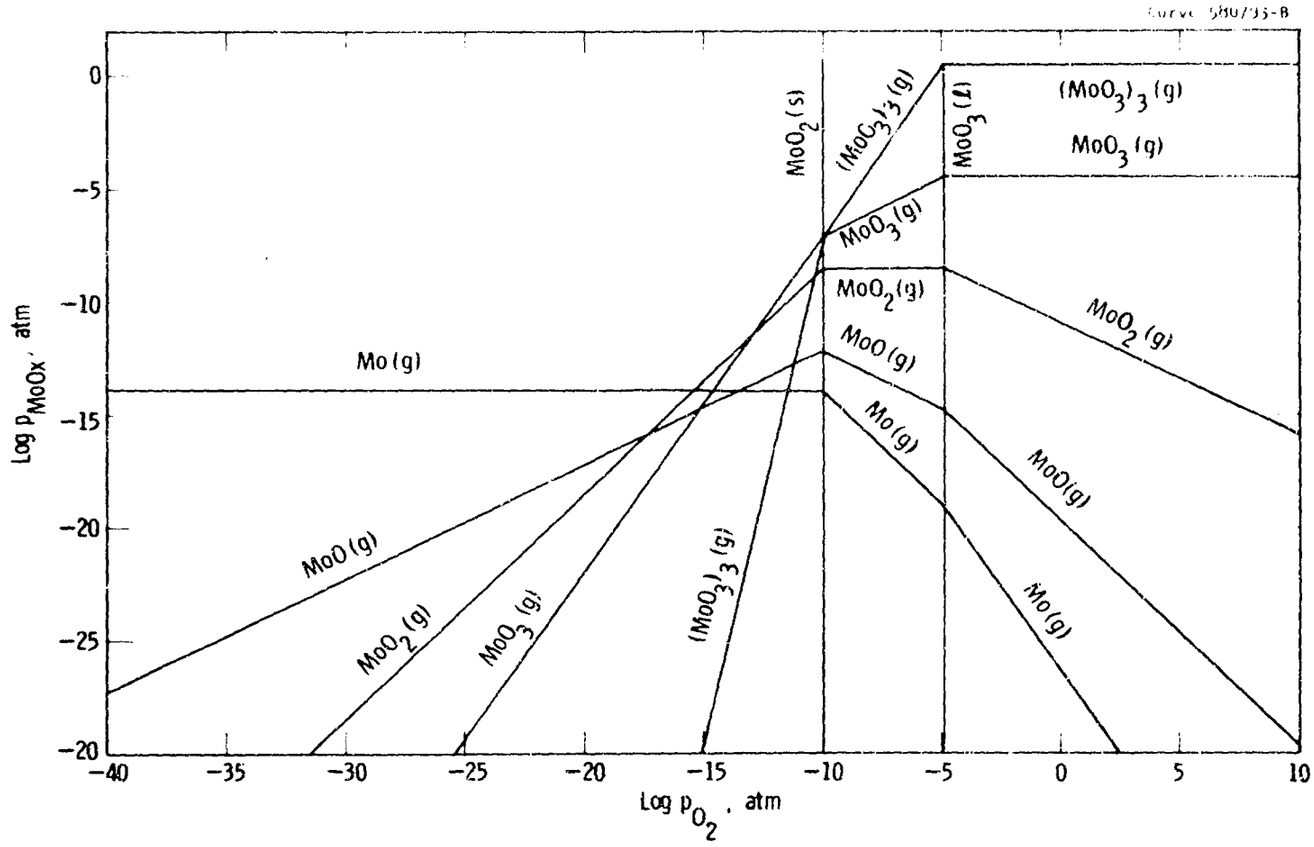

Fig. 14—Thermochemical data - oxidation of molybdenum, 1600°K

Since gas flow and quenching conditions are present in many reaction systems, the equilibrium conditions indicated in Table 7 and in Figures 11-14 may not be reached. Electron diffraction studies on the oxidation of molybdenum show that $MoO_2(s)$ is the major oxide in the surface layer. $MoO_3(s,l)$ is removed leaving $MoO_2(s)$ on the surface layer. At 1600°K $MoO_2(s)$ will remain on the surface at an oxygen pressure of log $p_{O_2} > -15.4$. The oxide pressure log $p_{MoO_2(g)} = -14.8$.

5. HIGH VOLTAGE ELECTRON DIFFRACTION APPARATUS FOR STUDYING OXIDATION REACTIONS AT PRESSURE, AT TEMPERATURE AND UNDER FLOW CONDITIONS

5.1 Introduction

One of the important problems in the chemical behavior of high temperature materials is the chemical composition and crystal structure of the surface undergoing reaction. This is especially true for the study of refractory metals where volatile oxides are formed. Models for the oxidation of refractory metals have been proposed without adequate information on the crystal structure of the reaction interface. High voltage electron diffraction is the only method for the evaluation of the surface crystal structure.

Recent studies at our laboratories and elsewhere have shown that high voltage electron diffraction using 250 kV energized electrons greatly improves the resolution of the diffraction patterns and the possibilities of extending the method.

This report will briefly describe the chief components of the 250 kV electron diffraction camera and a new special reaction chamber in the camera for studying reaction interfaces at temperature, in the presence of a gas atmosphere and under flow conditions. Preliminary studies have been made on the oxidation of molybdenum at temperatures of 900° to 1300°C and at pressures of 10^{-1} torr under flow conditions.

Commercial electron microscopes and electron diffraction cameras operate with accelerating voltages of 50-150 kV. A number of higher voltage instruments have been built in England, France and Japan.

The relative advantages of higher voltage electron beams have been discussed by Finch, Lewis and Webb[18] in 1953 and by several Japanese workers.[19][20]

The advantages of increasing the beam potential are: (1) greater transmission of electrons through thick specimens, (2) smaller adsorption of energy from the beam, (3) larger ratio of elastically to inelastically scattered electrons, (4) smaller disturbances occur in the diffraction patterns due to electrical charging of the specimen and (5) decrease in depth of penetration of the specimen by the electrons. These factors improve (1) the contrast of the diffraction pattern, (2) the conditions for taking meaningful diffraction patterns and (3) the design considerations for the construction of internal reaction chambers for studying chemical reactions "in situ".

5.2 Electron Diffraction Camera

A brief description of the apparatus will be given. The instrument was designed for electron beam voltages up to 250 kV. Many parts of an older 50 kV camera were used in the new instrument. This limited the vacuum in the system and the basic electron optics. One of the major tasks was the development of a maintenance free electron gun. A 300 kV "Sames" D.C. voltage source and controlled D.C. power sources for the electron lenses, deflecting plates, and tilt coils were purchased. The electron gun, main column, condenser lens system, and x-ray shielding system were built in our laboratories. To minimize

---

18. G. I. Finch, H. C. Lewis and D.P.D. Webb, Proceedings of the Physical Society, B, Vol. LXVI, 949 (1953).
19. B. Tadano, Y. Sakaki, S. Maruse and N. Morito, J. of Electron-microscopy, Vol. 4 (Annual Edition) 1956.
20. H. Watanabe, S. Nagakura and N. Kato, Proceedings of First Regional Conference in Asia and Oceania, Tokyo, 1956.

contamination and high voltage breakdown problems, a new high vacuum pumping system was built.

Continuing our program, we recently built a reaction chamber furnace assembly and auxiliary gas handling apparatus for the study of high temperature gas-metal reactions "in situ".

Figure 15 shows a simplified schematic drawing of the several sections of the instrument. The 3-stage electron gun, voltage divider, and battery operated filament source are shown at the top of Figure 15. The two stage condensing lens system, electron beam tilt system and beam deflection system are shown in the center. The reaction chamber, furnace system and specimen support system, and the fluorescent screen and film chamber are shown at the bottom of Figure 15. Two liquid nitrogen cold traps are incorporated in the apparatus, the first is in the section below the specimen while the second is located adjacent to the condenser lenses and in the pumping line.

The three stage gun is enclosed in an acrylic plastic box surrounded by a uni-potential hemisphere. The air within the box is dried to prevent electrical breakdowns under moist atmospheric conditions. Voltage breakdowns have been minimized by equalizing the high voltage fields along the ceramic tube through the use of corona rings and by eliminating electrical stress points in the gun and in the voltage divider.

Below the electron gun four electromagnetic tilt coils are mounted at 90° intervals. The coils are used to align the beam in the column.

A double condenser lens system is used for controlling the beam size and beam intensity. Below the lower condenser or focusing lens is a system of deflection plates for manipulation of the beam in the X-Y plane on the fluorescent screen.

A "Sames" 300 kV D.C. 1 m.a. high voltage source is used. This unit has a ripple of 1% root mean square and a drift of 0.5% for

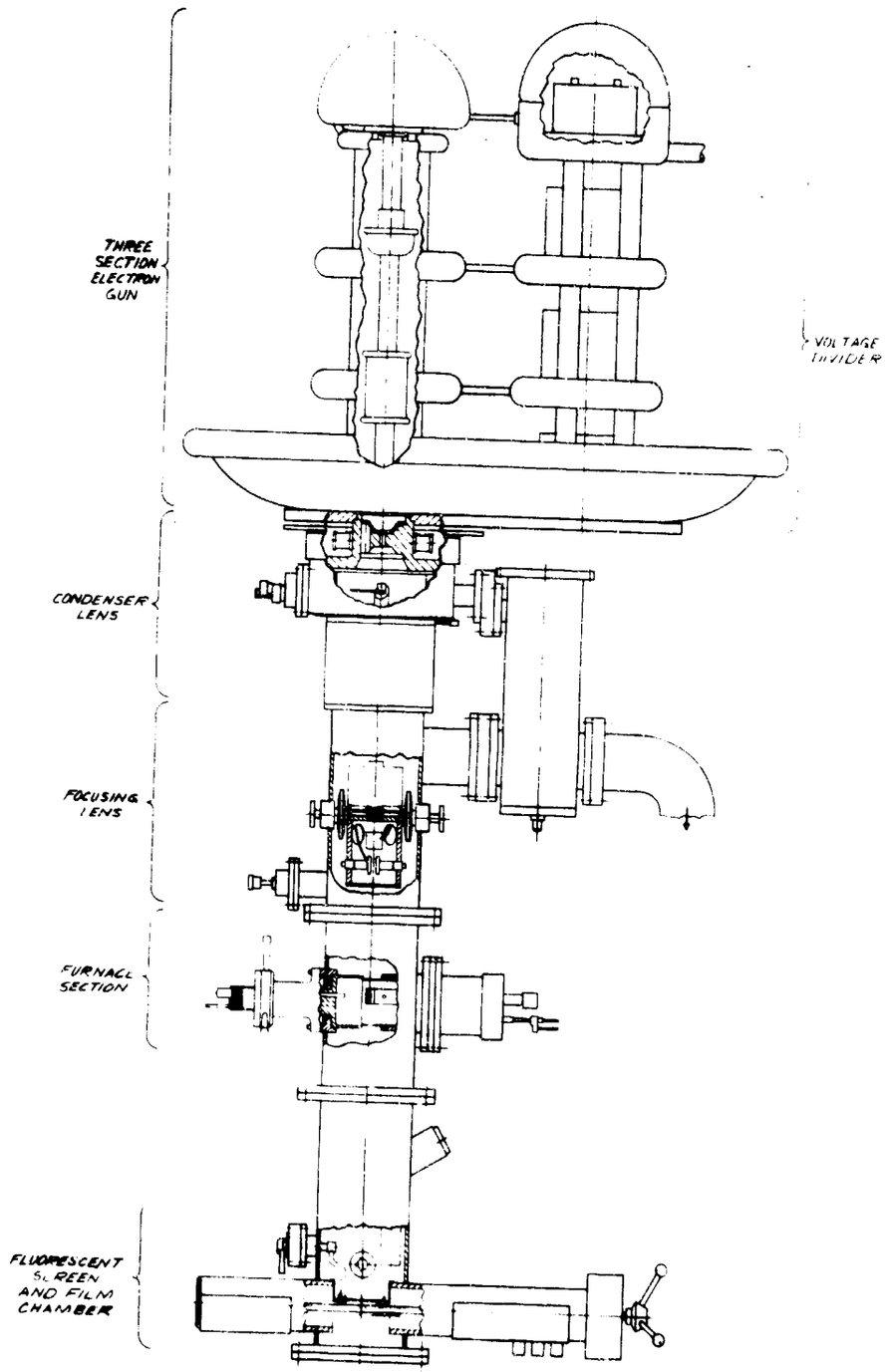

ELECTRON DIFFRACTION APPARATUS
FIG 15

4880 D60

a 5% change in line voltage. A 2 volt lead acid battery is enclosed in a polished aluminum corona dome to provide power for operating the tungsten filament electron source. All of the D.C. power sources for energizing the electron lenses, tilt controls, and deflection plates have stabilized solid state circuits.

5.3 Strip Heater Furnace and Reaction Chamber

Figure 16 shows details of the furnace and reaction chamber which was developed for electron diffraction study of chemical reactions "in situ" at temperature, pressure, and under flow. The metal specimen in the form of a strip .6 cm wide, 0.01 cm thick and 3.5 cm long is mounted under tension. Current is supplied to the strip by means of water cooled insulated leads. The strip can be moved in and out of the beam and tilted so as to vary the proper grazing angle. The specimen and specimen holder can be isolated from the camera by closing the two sections. Two apertures in the chamber are used to allow the electron beam to impinge on the specimen and to allow the diffracted electrons to pass out of the reaction chamber and on to the fluorescent screen and photographic plate.

Figure 17 shows a schematic diagram of the gas handling system. The furnace chamber at the right is shown in the closed position. Oxygen or other gases can be directed through a tube to the center of the heated sample. The gases can be removed by using an auxiliary pump or by pumping through the aperture into the main column of the diffraction camera. Using the apertures alone it is possible, by controlling the leak valve, to operate the furnace chamber at 10^{-1} torr and the column at 10^{-4} torr. The flow rate is determined by observations of the pressure on a calibrated reservoir. The pressure in the gas inlet line is read by sensitive capacity manometer. Pressure at the inlet line can be controlled from 10^{-4} torr to 10^{-1} torr.

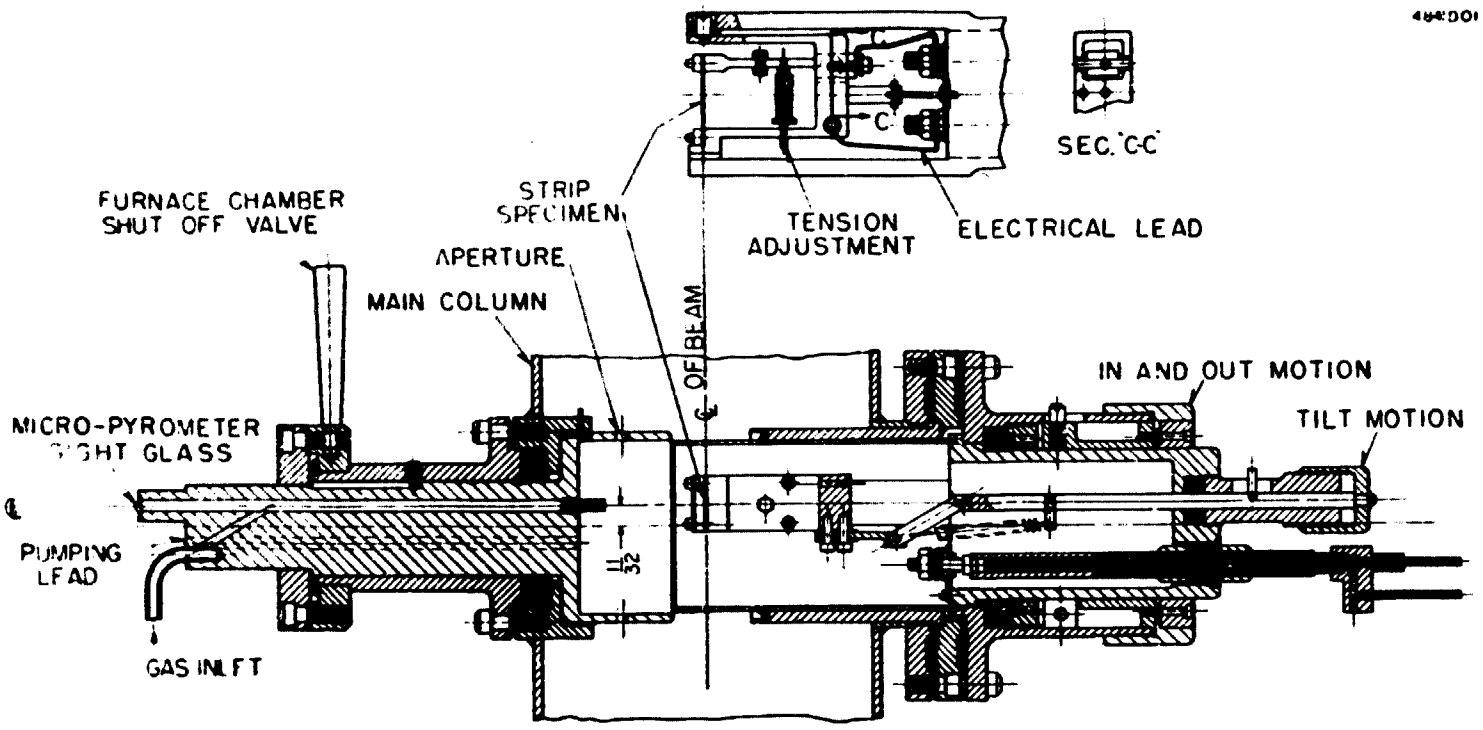

STRIP RESISTANCE FURNACE FOR
ELECTRON DIFFRACTION CAMERA
FIG. 16

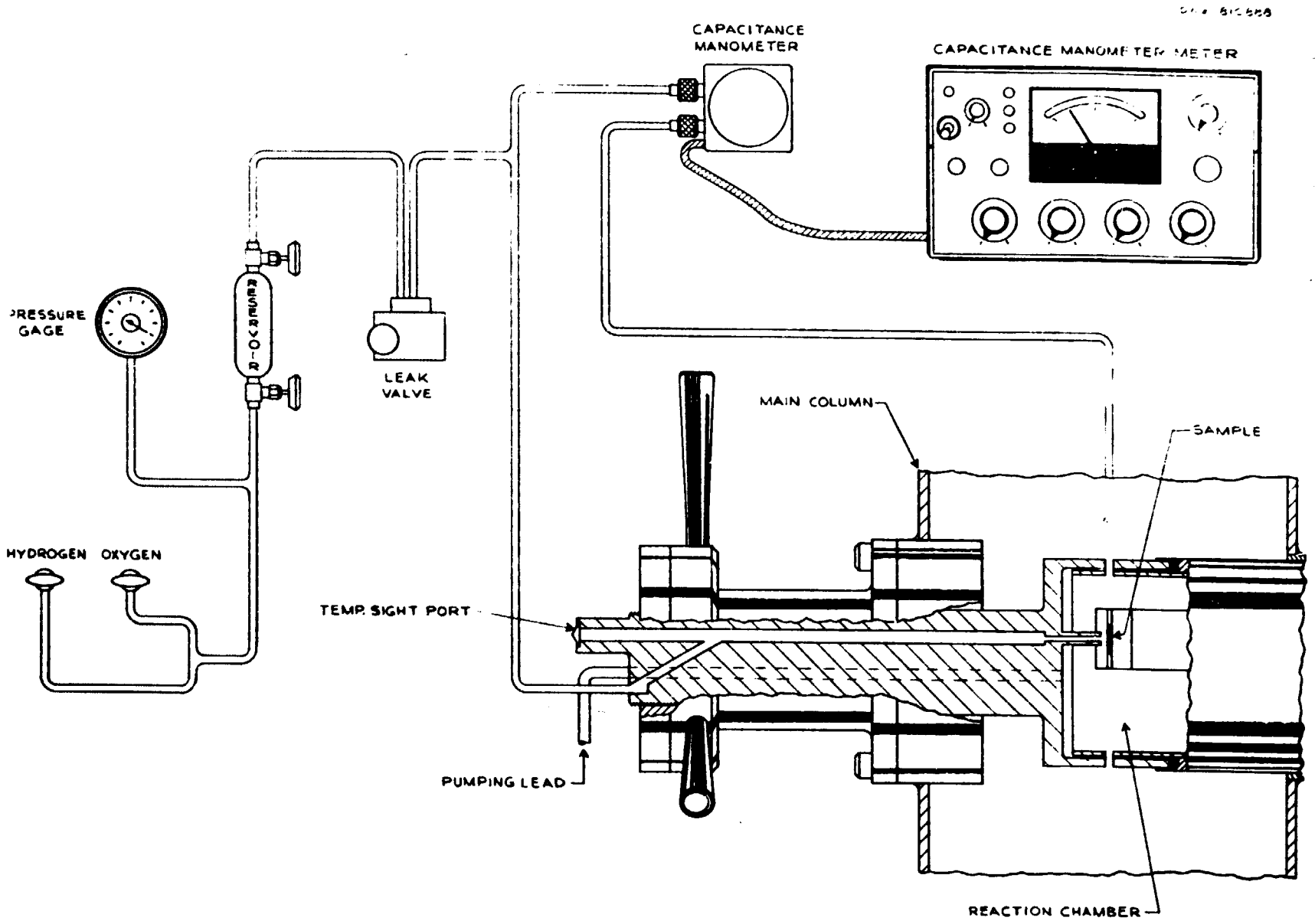

FIG. 17 - ELECTRON DIFFRACTION GAS HANDLING SYSTEM

5.4 Test of Gas Handling System

Tests were made on the flow rate of oxygen molecules in the reaction system using the apertures system for pumping into the column. Table 8 shows the calculated flow rates and an estimate on the rate of reaction of molybdenum based on a 100% flow efficiency and a 1 cm^2 reaction area. At a pressure of 10^{-1} torr at the inlet line, a flow rate of 5.8×10^{17} molecules of O_2/sec was observed. The flow velocity through the 2 mm diameter orifice was 6000 cm/sec.

5.5 Determination of Instrument Constant

Zinc oxide and magnesium oxide smokes were used as comparison standards to calibrate the electron diffraction camera since the accelerating voltage could vary from day to day. For most precise work the comparison standard diffraction pattern is taken at the same time as the unknown diffraction pattern.

The instrument constant for transmission patterns is given by the equation $K_T = D_{hkl} \times d_{hkl}$. Here D_{hkl} is the diameter of the ring for a given lattice spacing, d_{hkl}. The instrument constant for reflection patterns is given by the equation $K_R = R_{hkl} \times d_{hkl}$. Here R_{hkl} is the radius of the half rings for a given lattice spacing, d_{hkl}. This constant is calculated for each ring and an average value determined. The best calibrating materials should give 10 or more sharp diffraction rings An accuracy of about 0.3 percent was obtained for reflection patterns and about 0.2 percent for transmission patterns. The instrument constant K_T for transmission determined from an MgO pattern was 1.920 cm-Å. The instrument constant for reflection also determined from MgO was 0.950 cm-Å. The specimen to plate distance was different for reflection and transmission. This accounts for the fact that K_T is not $2 \times K_R$.

Table 8

Flow Rates and Estimated Reaction Rates for
Electron Diffraction Reaction System

Pressure** torr	Δ P torr/sec	cc torr O_2/sec	Molecules O_2/sec	Estimated Rates of Reaction*	
				atoms Mo/sec	Å/sec (1 cm^2)
0.1	0.5	18	5.8×10^{17}	3.9×10^{17}	600
0.01	0.05	1.8	5.8×10^{16}	3.9×10^{16}	60

*Based on 100% flow efficiency and 1 cm^2 area

**Pressure measured in gas inlet line

5.6 Results

5.6.1 Test Study on Rhombohedral α-Fe_2O_3

To evaluate the electron diffraction camera an electron diffraction pattern was taken of high purity α-Fe_2O_3 obtained from Dr. M. Bloom of the Naval Research Laboratories. A transmission pattern was taken of the powder dispersed on a thin Parlodion film. Table 9 shows the calculated d_{hkl} values and intensities together with literature values obtained from an x-ray diffraction study.[21] The d_{hkl} values are in excellent agreement. Many more reflections could be obtained from the pattern. However, the d_{hkl} values were not tabulated from the literature source. d_{hkl} values as low as 0.5 can be obtained with the high voltage electron diffraction camera. These values are of special use for lattice parameter studies.

5.6.2 Study of Molybdenum Oxidation

Table 10 shows the results of a study on the oxidation of molybdenum at various temperatures using a flow rate of 5.8×10^{17} O_2 molecules/sec. The pressure in the gas inlet tube was 0.1 torr. Patterns were taken in the following sequence: in the vacuum of the camera before reaction, at reaction times of 1, 5, and 15 minutes, and in vacuum after oxidation. MoO_2 was the predominant oxide found. At 1300°C single crystal diffraction spots of 3 molybdenum crystals were observed and diffraction rings of an unidentified structure. The spot patterns were indexed as molybdenum.

The crystal structure studies suggest that MoO_2 and possibly $MoO_{2.75}$ exist on the surface during oxidation. Molybdenum does not oxidize to volatile oxides directly from bare metal surface. The MoO_2 or $MoO_{2.75}$ oxide film is sufficiently thick to give a good electron diffraction pattern.

---

21. ASTM X-ray diffraction data card 13-534.

Table 9

Comparison Electron Diffraction Pattern with Literature

Rhombohedral α-Fe_2O_3

α-Fe_2O_3 Experimental		α-Fe_2O_3
I/I_o	d_{hkl}	d_{hkl} literature[21]
5	3.651	3.680
10	2.698	2.697
10	2.509	2.516
10	2.201	2.205
7	1.832	1.840
10	1.692	1.693
4	1.592	1.598
6 Diffuse	1.485	1.485
6 Diffuse	1.451	1.453
		1.349 v.w.
6	1.303	1.310
	-	1.258 v.w.
	-	1.227 v.w.
2 Diffuse	1.203	1.189
2 Diffuse	1.186	N.G.
2 Diffuse	1.102	N.G.
3 Diffuse	1.046	N.G.

v.w. Very weak

N.G. Not given

Table 10

Oxides Formed on Molybdenum at Temperatures and in Gas Flow of 5.8×10^{17} O_2 molecules/sec.

Reaction Conditions			
Temp. °C	Pressure torr	Time min.	Oxides
900	vac	0	$MoO_{2.75}$
	0.1	1	MoO_2
	0.1	5	MoO_2
	0.1	15	MoO_2
	vac	wait 10 min	MoO_2
1000	vac	0	MoO_2
	0.1	1	MoO_2
	0.1	5	MoO_2
	0.1	15	$MoO_{2.75}$
	vac	wait 10 min	MoO_2
1100	vac	0	Mo + MoO
	0.1	1	MoO_2
	0.1	5	MoO_2
	0.1	15	MoO_2
	vac	wait 10 min	MoO_2
1200	vac	0	MoO_2
	0.1	1	MoO_2
	0.1	5	Mo + MoO_2
	vac	wait 10 min	Mo + MoO_2
1300	vac	0	Unidentified structure
	0.1	1	Mo + Unidentified structure
	0.1	5	Mo + Unidentified structure
	vac	wait 5 min	Mo + Unidentified structure

Two mechanisms of reaction can be suggested: (1) Molybdenum atoms diffuse through the oxide film of MoO_2 to the surface where reaction occurs with oxygen to form $(MoO_3)_3$. (2) Some of the oxygen diffuses through the oxide film to form MoO_2 at the metal oxide interface. The remainder of the oxygen reacts with MoO_2 solid to form MoO_3 which volatilizes.

The formation of unidentified structures on the surface is not unexpected if small quantities of impurities which form non-volatile oxides are in the metal. Consider the case of a 0.01 percent iron impurity and assume the maximum rate of reaction 600 Å/sec. After 15 minutes or 900 seconds one would have 540,000 Å of molybdenum reacted with 54 Å of iron remaining on the surface to form an oxide film of iron.

6. SUMMARIES OF RECENT SCIENTIFIC PAPERS

6.1 The Graphite-Hydrogen Reactions and Their Implications in Geochemistry, E. A. Gulbransen, Nature 212, 1420 (1966).

The reaction of graphite with hydrogen at high temperature and low pressure under rapid quenching conditions was studied using levitation heating and mass spectrometric analyses of the reaction products. Small quantities of methane, ethylene, acetylene, benzene, and toluene were formed. Thermochemical analyses suggests that no appreciable reactions should occur. In one experiment at 1400°C and 10 torr hydrogen pressure, 0.34 mole percent methane, 0.11 ethane, 0.21 ethylene, and 0.17 benzene were formed in a two minute heat.

These results are of interest not only in high temperature chemistry of materials but also in geochemistry. Reactions of this type could have occurred at an early stage in the formation of the earth's atmosphere, hydrosphere, and lithosphere.

6.2 Nature of the Reaction Products Formed in the Graphite-Hydrogen Reaction at 1300°-1400°C, E. A. Gulbransen and W. M. Hickam, J. Electrochemical Technology 5, 5-6 (1967).

Graphite has been shown to react with hydrogen at elevated temperature, however the reaction products are unstable. A special system of small volume with levitation heating of the specimen and a mass spectrometer was used to study the nature of the reaction products. At 1300°-1400°C and at pressures of 5×10^{-2} to 400 torr, methane, ethylene, acetylene, benzene, and toluene were the major hydrocarbons

formed. Calculations from kinetic data suggest that only a small fraction of the reaction products are observed due to inadequate quenching and to the inherent instability of the hydrocarbons. The graphite-hydrogen reaction is an example of a chemical reaction proceeding under conditions where the reaction products are unstable.

6.3 Oxidation of Silicon at High Temperature and Low Pressures under Flow Conditions and the Vapor Pressure of Silicon, E. A. Gulbransen, K. F. Andrew and F. A. Brassart, J. Electrochem. Soc. 113, 8, 834 (1966).

Wagner has predicted from thermochemical and diffusion theory analyses that silicon may react actively or passively with oxygen at high temperature depending on the oxygen pressure. To determine the characteristics of the oxidation reaction for these reaction conditions, a kinetic study was made at temperatures between 1100° and 1300°C and pressures of 9×10^{-3}, 4×10^{-2}, and 1×10^{-1} torr using a dynamic reaction system. Very fast reactions were found where predicted. At 10^{-1} torr and 1200°C, an oxidation rate of 3.7×10^{18} silicon atoms per cm^2-second was observed. This was 7100 Å of silicon reacting per second. The rates of oxidation were nearly independent of temperature, but were a linear function of gas flow or pressure. Flow efficiencies of over 70% were found for the 9×10^{-3} torr pressure runs.

Several conclusions were made from the kinetic studies. (A) Gas diffusion processes were rate controlling for the conditions of the reaction; (B) Silicon reacted completely with oxygen under the conditions with only trace amounts of silica as residues; (C) Maximum oxygen pressure for maintaining oxide free surfaces were increased by the imposition of flow on the reaction; (D) Extreme care must be used to avoid contamination of the gas source or system with gases containing carbon; (E) The rate of oxidation was a direct function of flow or gas pressure.

6.4 Oxidation of Silicon Carbide at 1150° to 1400°C and at 9×10^{-3} to 5×10^{-1} torr Oxygen Pressure, E. A. Gulbransen, K. F. Andrew and F. A. Brassart, J. Electrochem. Soc. 113, 12, 1311 (1966).

A kinetic study was made of the oxidation of high-purity silicon carbide using a dynamic-type reaction system. Two types of oxidation behavior were found. Passive oxidation occurred for conditions where silica films were formed on the surface. Active oxidation occurred for conditions where volatile silicon monoxide was formed. The transition conditions between the two types of oxidation were studied as a function of oxygen pressure and temperature. The transition temperatures and pressures were related to thermochemical conditions for the reaction of silicon carbide with silica to form silicon monoxide and carbon monoxide. Kinetic theory efficiencies up to 123% were calculated for the active region of oxidation.

7. PUBLICATIONS AND REPORTS

STUDIES ON THE HIGH TEMPERATURE OXIDATION OF MOLYBDENUM, TUNGSTEN, NIOBIUM, TANTALUM, TITANIUM AND ZIRCONIUM

Project Number: ARO-D-196

Contract Number: DA-31-124-ARO-D-196

Progress Report No. 1 - Period covered: March 19, 1964 to September 30, 1964

Progress Report No. 2 - Period covered: October 1, 1964 to March 31, 1965

Progress Report No. 3 - Period covered: April 1, 1965 to September 30, 1965

Progress Report No. 4 - Period covered: October 1, 1965 to March 31, 1966

Progress Report No. 5 - Period covered: April 1, 1966 to September 30, 1966

These reports were submitted to: Metallurgy and Ceramics Division, U.S. Army Research Office, Durham, North Carolina 27706.

Oxidation of Silicon at High Temperatures and Low Pressures under Flow Conditions and the Vapor Pressure of Silicon. E. A. Gulbransen, K. F. Andrew and F. A. Brassart. J. Electrochem. Soc. 113, No. 8, 834 (1966).

Oxidation of Silicon Carbide at 1150° to 1400°C and at 9×10^{-3} to 5×10^{-1} Torr. E. A. Gulbransen, K. F. Andrew and F. A. Brassart. J. Electrochem. Soc. 113, No. 12 (1966).

High Temperature Oxidation in Flow Reaction Systems. E. A. Gulbransen, K. F. Andrew and F. A. Brassart. To be published - Proceedings of 3rd International Congress on Metallic Corrosion, Moscow, USSR (1966).

The Graphite-Hydrogen Reactions and Their Implications in Geochemistry. E. A. Gulbransen. Nature 212, 1420 (1966).

Nature of the Reaction Products Formed in the Graphite-Hydrogen Reaction at 1300°-1400°C. E. A. Gulbransen and W. M. Hickam. J. Electrochemical Technology 5, 5-6 (1967).

8. PARTICIPATING SCIENTIFIC PERSONNEL

Mr. Fred A. Brassart, Associate Engineer

Mr. Kenneth F. Andrew, Research Engineer

Dr. Earl A. Gulbransen, Consulting Scientist

F. A. Brassart
Physical Chemistry R&D

K. F. Andrew
Physical Chemistry R&D

E. A. Gulbransen
Physical Chemistry R&D

Approved: W. T. Lindsay, Jr., Manager
Physical Chemistry R&D

Unclassified
Security Classification

DOCUMENT CONTROL DATA - R&D

(Security classification of title, body of abstract and indexing annotation must be entered when the overall report is classified)

1. ORIGINATING ACTIVITY *(Corporate author)* Westinghouse Electric Corporation	2a. REPORT SECURITY CLASSIFICATION Unclassified 2b. GROUP NA

3. REPORT TITLE

STUDIES ON THE HIGH TEMPERATURE OXIDATION OF MOLYBDENUM, TUNGSTEN, NIOBIUM, TANTALUM, TITANIUM, AND ZIRCONIUM

4. DESCRIPTIVE NOTES *(Type of report and inclusive dates)*

Final Report

5. AUTHOR(S) *(Last name, first name, initial)*

Gulbransen, E. A.
Andrew, K. F.
Brassart, F. A.

6. REPORT DATE	7a. TOTAL NO. OF PAGES	7b. NO. OF REFS
April 18, 1967	63	21

8a. CONTRACT OR GRANT NO. DA-31-124-ARO-D-196 b. PROJECT NO. 20014501B32D c. d.	9a. ORIGINATOR'S REPORT NUMBER(S) 9b. OTHER REPORT NO(S) *(Any other numbers that may be assigned this report)* 4067.3-MC

10. AVAILABILITY/LIMITATION NOTICES

Distribution of this report is unlimited.

11. SUPPLEMENTARY NOTES	12. SPONSORING MILITARY ACTIVITY
None	U.S. Army Research Office-Durham Box CM, Duke Station ~~Durham, North Carolina 27706~~

13. ABSTRACT

The purpose of these studies was twofold: (1) to extend and develop vacuum microbalance and electron diffraction methods for studying fast oxidation reactions of high temperature metals and solids under carefully controlled conditions of temperature, pressure, and gas flow; and (2) to determine the kinetics and mechanisms of oxidation of a number of high temperature metals and solids.

14. KEY WORDS

oxidation resistance
tungsten
molybdenum
niobium
tantalum
titanium
zirconium
volatilized gases
kinetics of oxidation

DD FORM 1 JAN 64 1473

Unclassified
Security Classification